The role of microbial sulfate reduction in calcium carbonate polymorph selection

Chin Yik Lin[1], Alexandra V. Turchyn[1], Zvi Steiner[1], Pieter Bots[2], Giulio I. Lampronti[1], Nicholas J. Tosca[3]

[1]Department of Earth Sciences, University of Cambridge, Downing Street, Cambridge CB2 3EQ, United Kingdom.

[2]Department of Civil and Environmental Engineering, University of Strathclyde, Glasgow G11XJ, United Kingdom.

[3]Department of Earth Sciences, University of Oxford, South Parks Road, Oxford OX1 3AN, United Kingdom.

ABSTRACT

Microbial sulfate reduction is a dominant metabolism in many marine sedimentary environments. The influence of this metabolism on the kinetics of $CaCO_3$ growth, as well as the dominant polymorphs precipitated, is poorly understood. To investigate the role of microbial metabolism on $CaCO_3$ precipitation and polymorph selection, we conducted growth experiments with the sulfate reducing bacteria (*D. bizertensis*) in media with varying Mg/Ca and different seeding materials (calcite and kaolinite). Our results suggest that sulfate reducing bacteria both induce carbonate mineral precipitation through an increase in alkalinity and serve as a nucleation sites for the growing carbonate mineral; the majority of the carbonate minerals produced were on cell material rather than mineral seeds. We also find the Mg/Ca and presence of phosphate in the media play a key role in controlling the rates of carbonate mineral precipitation and calcium carbonate polymorph selection. In media where the Mg/Ca is greater than 2, crystalline monohydrocalcite (MHC) is the primary carbonate mineral produced. Although phosphate concentrations have a lesser effect on which polymorph initially precipitates, a series of abiotic and transformation experiments suggests that the presence of phosphate stabilizes MHC crystals and prevents its transformation to more stable calcium carbonate polymorphs. Collectively, these results suggest that the polymorph of microbially-mediated calcium carbonate cements is determined by the solution chemistry upon nucleation.

Keywords: monohydrocalcite; Mg/Ca, seeding material, phosphate, transformation, sulfate reducing bacteria, incubation, inhibitors, nucleation

1.0 INTRODUCTION

Microbial sulfate reduction, coupled either to organic matter oxidation or anaerobic methane oxidation, is one of the key microbial reactions driving sedimentary carbonate formation in marine sediments, intertidal marshes, and hypersaline lakes (Berner et al., 1970; Pye et al., 1990; Coleman et al., 1993; Visscher et al., 2000; Warthmann et al., 2000; Raiswell and Fisher, 2004; Baumgartner et al., 2009; Gallagher et al., 2012; Meister, 2013). Microbial sulfate reduction, particularly followed by precipitation of sedimentary pyrite, raises pH and increases alkalinity, while the negatively charged bacterial cell surface can serve as a nucleation surface for carbonate/mineral growth (van Lith, 2001; Bosak and Newman, 2005; Visscher and Stolz, 2005; Aloisi et al., 2006; Wacey et al., 2007; Zhu and Dittrich, 2016; Picard et al., 2018). The production of exopolymeric substances (EPS) around the bacterial cells also aids the nucleation and subsequent precipitation of calcium carbonate (Kawaguchi and Decho, 2002; Braissant et al., 2007; Dupraz et al., 2009; Obst et al., 2009; Tourney and Ngwenya, 2009). Despite work on the process of microbially-induced carbonate mineral precipitation, our understanding of how microbial sulfate reduction influences calcium carbonate mineralization and the formation of various calcium carbonate polymorphs remains limited. The vast majority of studies exploring the formation of different calcium carbonate polymorphs have focused on abiotic precipitation experiments, despite the fact that the majority of natural calcium carbonate mineral precipitation is biologically controlled.

The earliest studies on the nucleation, crystallization, and transformation of various calcium carbonate polymorphs focused largely on the precipitation of aragonite versus calcite and the role of magnesium ions and Mg/Ca ratio of the solution (Katz, 1973; Berner, 1975; Burton, 1993; Ries et al., 2008; Smeets et al., 2015). It was initially shown that the precipitation of aragonite is favoured in a high ionic strength solution with high Mg/Ca ratio (Mg/Ca > 1), while calcite is favoured in solutions with a lower Mg/Ca ratio (Mg/Ca < 1). The important role of magnesium in promoting different calcium carbonate polymorphs derives from the fact that magnesium possesses greater hydration energy and therefore promotes

the formation of hydrous carbonate phases (Christ and Hostetle, 1970; Lippman, 1973; Ries et al., 2008; de Choudens-Sanchez and Gonzalez, 2009; Politi et al., 2009; Tommaso and de Leeuw, 2010; Hopkinson et al., 2012; Nishiyama et al., 2013; Blue et al., 2017). In addition, there is also a fundamental energetic barrier imposed by magnesium substitution for calcium in the calcite lattice, which may in part kinetically inhibit the formation of Mg-rich calcium carbonate minerals (Elstnerova et al., 2010; Xu et al., 2013).

Most inorganic precipitation studies also show that if the initial calcium carbonate precipitate is metastable (e.g. amorphous calcium carbonate and monohydrocalcite (MHC)), it will transform to calcite or aragonite over time via the Ostwald step rule and/or other non-classical nucleation pathways (Munemoto and Fukushi, 2008; Bots et al., 2012; Liu et al., 2013; Rodriguez-Blanco et al., 2014; De Yoreo et al., 2015). However, the transformation mechanisms of amorphous calcium carbonate or MHC in natural environments are still poorly understood (Stoffers and Fischbeck, 1974; Dahl and Buchardt, 2006; Nishiyama et al., 2013; Ihli et al., 2014; Munemoto et al., 2014; Wolf et al., 2015; Meic et al., 2017). To constrain the behavior of these transient intermediate polymorphs, laboratory studies have been performed under both dry and wet conditions (Marschner, 1969; Hull and Turnbull, 1973; Kamiya et al., 1977; Dejehet et al., 1999; Liu et al., 2013). MHC has been reported to transform to aragonite in a heated atmosphere (Brooks et al., 1950; Kamiya et al., 1977), to calcite in a magnesium-free medium (Taylor, 1975) and to aragonite in media with $Mg^{2+}/(Ca^{2+} + Mg^{2+})$ greater than 20 mol% (Munemoto and Fukushi, 2008). Although these inorganic and abiotic studies have highlighted several variables that can influence calcium carbonate mineralisation and polymorphism, microbial systems involve a number of interconnected processes that may affect mineralization in unanticipated ways. This may obscure the influence of specific metabolic processes on calcium carbonate formation in sediments, and the attendant biogeochemical consequences.

Understanding the dominant calcium carbonate polymorph produced through microbially-induced carbonate mineral precipitation is inherently more difficult because microbial metabolic byproducts and solution chemistry evolve over time. Within sedimentary pore fluids, for example, the concentrations of various elements that may promote or inhibit carbonate precipitation or play a role in the type of polymorph precipitated, may change

with depth and/or time. For example, dissolved phosphate concentrations, which have been shown to influence carbonate polymorphism, can range from 0 – 600 uM in sediment pore waters (Delaney, 1998; Burdige, 1991; Sasaki et al., 2001; Faul et al., 2005; Kraal et al., 2012; Sinkko et al., 2013; Stockmann et al., 2018). An unanswered question is whether during microbially-induced carbonate mineral formation there is a difference in the calcium carbonate polymorphs produced, relative to those found in the well-studied abiotic experiments. If so, what are the master variables that influence the stability field of the precipitating carbonate polymorph?

In this paper, we explore how microbial sulfate reduction influences calcium carbonate polymorphism using pure cultures of sulfate reducing bacteria under varying Mg/Ca and with different seeding materials. We also investigate the transformation of the microbially induced calcium carbonate polymorphs to more stable polymorphs under a range of geochemical conditions. Finally, we propose a stability field for calcium carbonate polymorphs obtained from our experiments and suggest the master variables that control the formation of microbially-induced calcium carbonate polymorphs.

2.0 EXPERIMENTAL

2.1 *Incubation* experiments

A pure culture of the sulfate reducing bacteria *Desulfovibrio bizertensis* (single bacteria strain) was used in all incubation experiments. The strain was purchased from Leibniz-Institut DSMZ-Deutche Sammlung von Mikroorganismen und Zellkulturen GmbH (DSMZ) DSM No. 18034. This strain was originally isolated from marine sediments in the Mediterranean Sea near Bizerte, Tunisia (Haouari et al., 2006). Our incubations were carried out in either 125 mL or 100 mL reaction vessels, tightly sealed with a blue butyl rubber stopper under strictly anoxic conditions. All experiments were performed at 25 ± 1°C in a water bath incubator. The incubation experiments were performed with different Mg/Ca (0:1, 1:1; 2:1, 3:1, 4:1 5.2:1; 9:1) including Atlantic seawater and artificial seawater and different seeding materials (kaolinite and calcite – see below).

2.2 *Composition of culture medium and inoculation*

The bacteria were initially cultured in Medium 163 as recommended by DSMZ (Supplementary A). An inoculum of the bacteria at stationary phase was transferred into the modified media and grown three times before the experiment began. The recipe for DSMZ medium 163 and the seawater medium used in this study are given in full in Supplementary Materials B. Artificial seawater was prepared using the Standard Practice for the Preparation of Substitute Ocean Water – Designation: D1141-98 (Reapproved 2013). Stock solutions of artificial seawater were freshly made from analytical grade (Analar) reagents and diluted to the desired Mg/Ca ratio. The seawater solution was heated to approximately 80 °C for two hours to degas O_2. Then, the solution was allowed to cool and the above chemicals were added except yeast extract. Formate (7.5 g L^{-1} or 110 mM HCOO-Na) was used as the sole electron donor in this study. Approximately 0.01% w/v of reductants (ascorbic acid and Na-thioglycolate), 4.0% w/v yeast extract and 1 mg L^{-1} resazurin (oxygen indicator) were added into both the Atlantic seawater and artificial seawater medium. About 80 mL of the solution was then decanted into smaller incubation vials with 0.3 g of seeding materials (such as calcite or kaolinite), crimp sealed and flushed with 90% N_2/10% CO_2 gas for 30 minutes. Finally, the medium was autoclaved for 15 minutes at 121°C. The sample medium was subsequently cooled to 25°C in the water bath before being inoculated. Yeast extract solution was added to the medium using a syringe filter (0.2 μm) before inoculation. Control samples were immediately re-autoclaved after inoculation to kill the bacteria, then placed into the water bath. All results from the control experiments are given in the supporting online material.

2.3 *Biotic incubation experiment*

Three sets of incubation experiments were undertaken with varying Mg/Ca and seeding materials (Table 1). Approximately 0.3 g of seeding material was used. Biotic incubation experiments were performed under quiescence (non-stirring) condition. Experiments were sampled every few days until carbonate precipitated – which was identified during the incubation based on a coincident decrease in pH and calcium concentration. Details of abiotic experiments are reported in Supplementary Material C.

Table 1: Summary of experiment setup for biotic incubation experiments.

Experiment	Mg^{2+} (mM)	Ca^{2+} (mM)	Mg/Ca	Seeds
K-0:1	0	10	0	Kaolinite
C-0:1	0	10	0	Calcite
K-0:2	0	20	0	Kaolinite
C-0:2	0	20	0	Calcite
K-1:1	10	10	1	Kaolinite
C-1:1	10	10	1	Calcite
K-2:2	20	20	1	Kaolinite
C-2:2	20	20	1	Calcite
K-3:3	30	30	1	Kaolinite
C-3:3	30	30	1	Calcite
K-4:4	40	40	1	Kaolinite
C-4:4	40	40	1	Calcite
K-2:1	20	10	2	Kaolinite
C-2:1	20	10	2	Calcite
K-3:1	30	10	3	Kaolinite
C-3:1	30	10	3	Calcite
K-4:1	40	10	4	Kaolinite
C-4:1	40	10	4	Calcite
K-Atl-SW	52	10	5.2	Kaolinite
C-Atl-SW	52	10	5.2	Calcite
K-9:1	90	10	9	Kaolinite
C-9:1	90	10	9	Calcite

2.4 *Aqueous sample analysis*

Media was collected from the sample bottle over the course of the experiments using a sterilized needle and syringe and without shaking the vials. Samples were filtered using a 0.2 μm filter and analyzed for alkalinity, sulfide concentration, major cations (calcium, magnesium, sodium, and potassium) and anions (sulfate and chloride). pH was measured at 25°C on the NBS scale using an Orion 3 Star meter with ROSS micro-electrode (ORION 8220 BNWP PerpHect ROSS – platinum wire as reference in iodine/potassium iodide solution, ROSS internal filling solution is 3M KCl). Samples for alkalinity, anions and cations were filtered through a 0.2 um syringe filter. Alkalinity was titrated potentiometrically with 0.1 M of HCl using a Metrohm 848 Titrino plus with error of 2.5%. The HCl used for titrations was standardized with certified reference material (CRM) 2.2298 meq/L. The CRM batch #157 used was provided by A.G. Dickson of Scripps Institution of Oceanography (Dickson et al., 2003).

An unfiltered sample was centrifuged at 900 rpm to separate any suspended solid in the solution before measurement for Optical density (OD) at 600 nm spectrum in a AquaMate Plus UV-VIS spectrophotometer. Phosphate concentrations were measured on the spectrophotometer using the molybdivanadophosphoric acid method (at 380 nm) described in Kitson and Mellon (1944).

Major cations and anions were diluted 20 times before measured using ion chromatography on a Dionex ICS-5000^{+} SP. The cation measurements were run with column IonPac AS18 and methanesulfonic acid (MSA 30mM) >99% as the eluent. The anions were passed through an anion column IonPac AG18 with 31mM of potassium hydroxide (KOH) as eluent. Calibration standards were prepared by dilution of OSIL Atlantic Seawater standard into 2%, 5% and 10% solution for all batch of analyses.

2.5 *Solid phase analysis*

The experiments were killed immediately after the final sampling. The sample (both solid and aqueous sample) were then decanted into a 50 mL falcon tube which was centrifuged at 5000 rpm for five minutes. Then, the aqueous samples were discarded. The remaining solid samples were carefully rinsed twice with MilliQ water and oven dried at 40°C overnight. Dried samples were powdered prior to mineralogical analysis through X-Ray Diffraction

(XRD). The dried samples were prepared by pipetting ~0.40 mL of an acetone smear containing the precipitate onto a zero-background holder. Samples were then kept in a clean cupboard while the acetone evaporated.

Powder X-ray diffraction was collected from Bruker diffractometers (see Supplementary Material D for details) Rietveld refinements were performed with the software Topas 4.1 (Coelho, 2007). Rietveld quantitative analysis is known to be unreliable for minor phases (<5 wt %) (McCusker et al., 1999). The accuracy is considered to be ± 1-2% for major phases, while the estimated standard deviation from the Rietveld calculation has no bearing on the accuracy or otherwise of the quantification itself, being merely related to the mathematical fit of the model (Madsen and Scarlett 2008). The dried precipitates were also analysed by field emission scanning electron microscopy (FESEM – QEMSCAN 650F FEI) equipped with an energy dispersive X-ray (EDX) detector to examine the morphology (secondary electron) and chemical composition (backscattered secondary electron) of the precipitates. The solid samples were placed on ultra-smooth carbon tape and sputter-coated with submicron layer (~10nm) of gold or carbon prior to SEM analysis.

2.6 *Monohydrocalcite transformation experiment*

To investigate the transformation and stability of monohydrocalcite initially formed in some experiments, we subjected the mineral to elevated temperatures in an aqueous solution. These experiments were designed to investigate possible final calcium carbonate polymorph. However, it should be recognized that the recrystallization pathway in the transformation experiment is different from the biotic experiment which performed under low temperature. Approximately 0.02 g of MHC was heated under different media in sealed bottles at 100°C for 48 hours (Munemoto and Fukushi, 2008; Liu et al., 2013). Two milliliters of the following media were used: (1) Atlantic seawater; (2) Mili-Q water; (3) Atlantic seawater with 4.0% w/v yeast extract added; and (4) Atlantic seawater with 750 µM inorganic phosphate (K_2HPO_4 – Molar mass: 174.2 g mol^{-1}). After heating, the media and the solid samples were separated by centrifugation at 4000 rpm for five minutes. The media was decanted and the remaining solids were rinsed with Mili-Q water and dried before analysis by XRD and scanning electron microscope as above.

2.7 *Saturation index and solution chemistry modelling*

PHREEQC (Parkhurst and Appelo, 1999) was used to evaluate the evolution of geochemistry during the experiments. The SIT database (*sit.dat*) was used to model the evolution of the aqueous geochemistry and to calculate the evolution of the saturation indices of the media with respect to relevant calcium carbonate polymorphs (i.e. calcite, vaterite, amorphous calcium carbonate (ACC) and monohydrocalcite (MHC)). The sit.dat uses the specific ion interaction theory to calculate activity coefficients to calculate saturation state in the media throughout the experiment (Brönsted, 1922; Guggenheim and Turgeon, 1955). The measured concentrations of sulfate and calcium ions were used to predict the evolution of the solution pH and alkalinity of the media at each sampling point. For these predictions we assumed that the decrease in the sulfate concentration was due to microbial sulfate reduction (Gallagher et al. 2012) and that the decrease in calcium concentrations was due to the precipitation of calcium carbonate. The modelled results for the pH and alkalinity were compared to the measured pH and alkalinity titrations to inform on the validity of the model described above. In the case of a large discrepancy between the modelled and measured alkalinity and pH, the alkalinity was adjusted in the model through the addition of $NaHCO_3$ to approximate the (de)sorption of carbonate ions from the kaolinite or calcite surfaces, and the pH was adjusted by the release of CO_2(g) to approximate (partial) equilibration with a low CO_2 headspace. The final results of the model were used to calculate the ion activity product (IAP: log a_{Ca2+} a_{CO32-}) to determine the saturation state with respect to ACC, which is log (IAP/K_{sp}) or log Ω (logK_{sp} = -6.40; Brecevic and Nielsen, 1989), monohydrocalcite (logK_{sp} = -7.60; Hull and Turnbull, 1973), vaterite (logK_{sp} = -7.90; Plummer and Busenberg, 1982), aragonite (logK_{sp} = -8.33; Plummer and Busenberg, 1982) and calcite (logK_{sp} = -8.48; Plummer and Busenberg, 1982).

3.0 RESULTS

3.1 *Evolution of aqueous chemistry*

The presented results are separated by the seeding material used in each experiment (kaolinite seeds versus calcite seeds). All killed controls and saturation indices for carbonate polymorphs other than MHC are presented in the Supplementary Materials E.

3.1.1 *Experiment with kaolinite seeds*

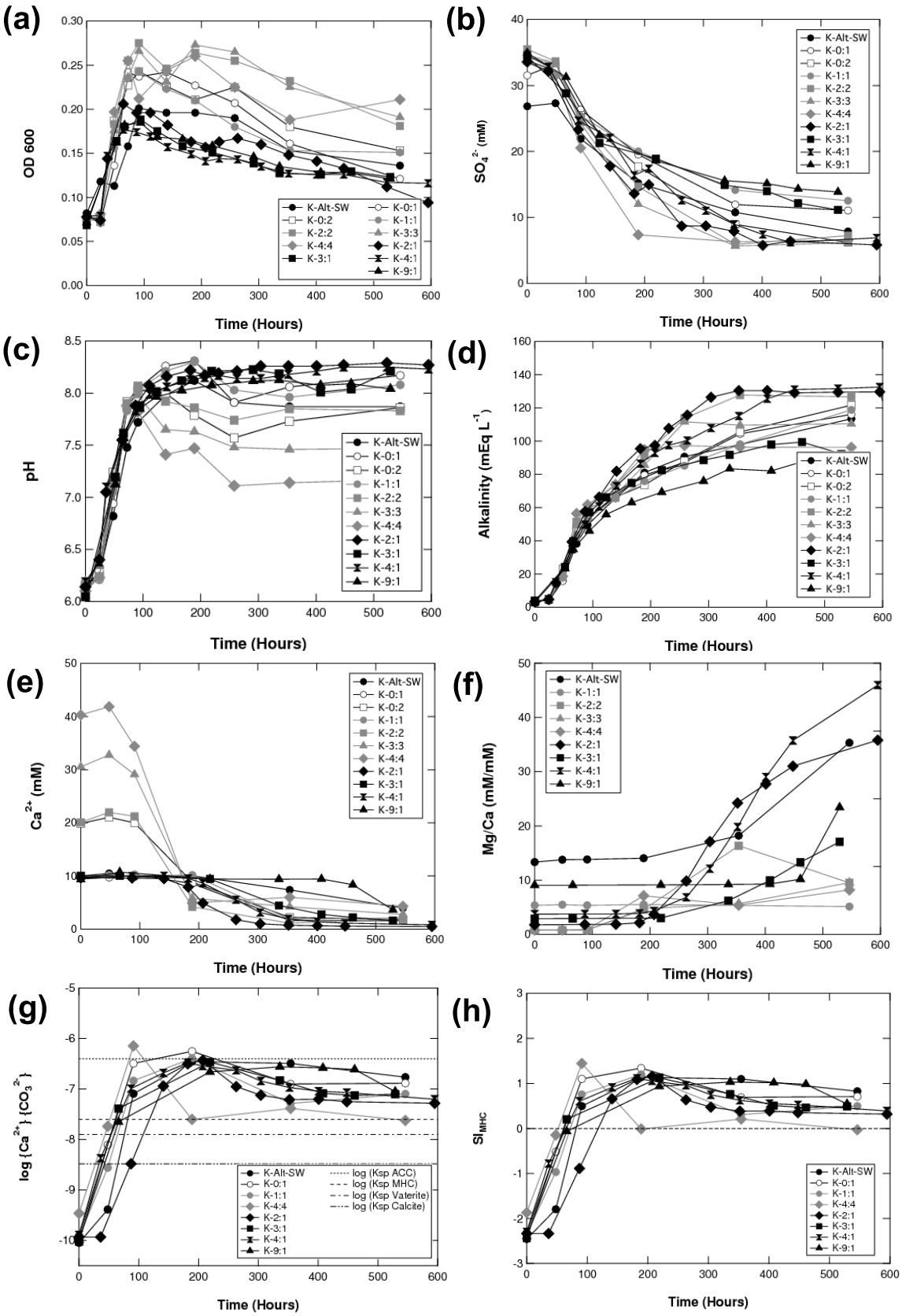

Figure 1: Aqueous chemistry data for the experiments with kaolinite seeds (a) optical density; (b) SO_4^{2-}; (c) pH; (d) total alkalinity; (e) Ca^{2+}; (f) Mg/Ca ratio; (g) ionic activity product for

$CaCO_3$; and (h) SI_{MHC} calculated immediately after inoculation until 546 hours. We did not observe any significant change in the killed samples (shown in supporting online material E).

Significant bacterial growth was observed in all incubated samples over the first 100 hours after which the bacteria reached a stationary phase (OD 600~0.15 – 0.25) (Figure 1a). Bacterial growth was not detected in the killed control samples (see Supplementary Material F). The pH in all incubated samples increases to ~8 as microbial sulfate reduction progressed (Figure 1 b and c). After 100 hours, carbonate mineral precipitation is observed in K-2:2, K-3:3 and K-4:4 (with Mg/Ca of 1 and magnesium and calcium concentrations at 20, 30 and 40mM, respectively). Experiments K-0:1 and K-1:1, with lower calcium concentrations, reached a higher pH before carbonate mineral precipitation started around 200 hours. A greater magnitude of pH drop (approximately 1 pH unit) is evident in K-4:4 compared to the other vials. Delayed precipitation of calcium carbonate was observed in seawater samples (K-Alt-SW). All experiments began with total alkalinity of approximately 4.0 ± 0.5 mEq L^{-1}, which then increased to greater than 100 mEq L^{-1}. The alkalinity for experiments K-2:2 and K-4:4 plateaus earlier (200 and 250 hours) relative to the other experiments (Figure 1d). The rate of calcium carbonate precipitation, as indicated by the decrease in the calcium concentration, increases with increasing initial calcium concentration (Figure 1e). Sulfate concentrations decrease over time, although they are never fully depleted. We note that the rate of sulfate depletion slows as carbonate minerals begin to precipitate. We observe a dramatic increase in the Mg/Ca ratio over time (Figure 1f). Samples with initial calcium concentration greater than 20 mM experienced a sharp increase in the saturation index or log Ω (saturation state) for all carbonate polymorphs at 100 hours. This increase in saturation index was most dramatic where the kaolinite seeded samples reached (or nearly reached) the K_{sp} of ACC. We observe that nearly double the amount of time is required for samples with 10 mM calcium to reach their highest ionic activity product (IAP) and precipitation started to slow down or stop when IAP started to drop (Figure 1g and h).

3.1.2 *Experiments with calcite seeds*

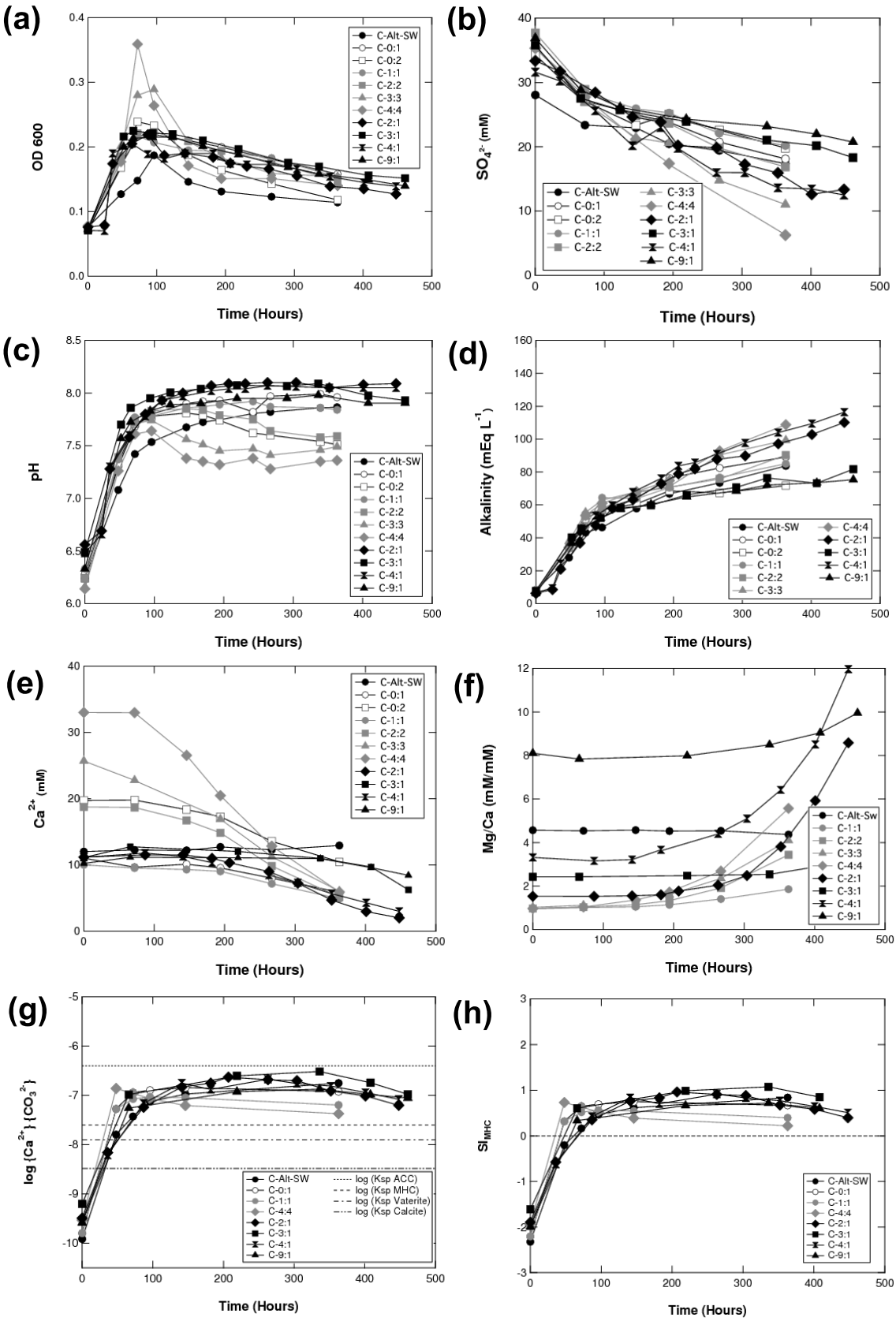

Figure 2: Aqueous chemistry data for the experiments with calcite seeds (a) optical density; (b) SO_4^{2-}; (c) pH; (d) total alkalinity; (e) Ca^{2+}; (f) Mg/Ca ratio; (g) ionic activity product for $CaCO_3$; and (h) SI_{MHC} measured immediately after inoculation until 546 hours. A drop in pH

and calcium concentrations in C-Alt-SW is not apparent although precipitation of MHC (measured by XRD and SEM) occurred.

Similar to experiments with kaolinite seeds, we observe a sharp rise in OD 600 and pH linked to microbial sulfate reduction within the first 100 hours (Figure 2a, b and c), which stabilizes and then gradually drops in the samples with Mg/Ca of 1 at higher absolute magnesium and calcium concentrations (C-3:3 and C-4:4). Although the experiment started at a lower pH of 6.2 – 6.5, the calcite seeds survived the first 50 hours of undersaturation (gravimetric data of calcite seeds presented in Table 6, Supplementary Material F). Total alkalinity increases to maximum values of 110 mEq L^{-1}, compared to the experiments with kaolinite seeds in which alkalinity increased to a maximum of 130 mEq L^{-1}. The concentration of phosphate, which is sourced from the yeast extract, was measured in this experiment (data shown in Supplementary Materials G) and initially ranged from 600 – 850 µM and gradually decreased by 50 to 500 µM as the experiment progressed. We observe a drop in calcium and sulfate concentration (Figure 2b and e), although at a lower rate than in the experiments with kaolinite seeds, and an increase in the Mg/Ca (Figure 2f). The K_{sp} for ACC in the experiment with calcite seeds is not reached (Figure 2g). The saturation index for the various calcium carbonate polymorphs (MHC, calcite, and aragonite) was lower than the saturation index with kaolinite seeds (Figure 2h and 1h) ($SI_{calcite}$, $SI_{aragonite}$, and $SI_{vaterite}$, are reported in Supplementary Materials E).

3.2 *Results from geochemical modelling*

PHREEQC was used both to calculate the SI for various carbonate polymorphs (Figures 1h and 2h) as well as to model the evolution of alkalinity over the experiment. In the alkalinity model, we note a greater discrepancy between the experimental and the modelled alkalinity in the experiments with kaolinite as seeding material (Figure 3a and c) than those with calcite as seeding material (Figure 3b and d). Despite the mismatch in some of the calcite seeding samples (Figure 3d), we were able to model most of the samples with good agreement between the measured and modelled alkalinity.

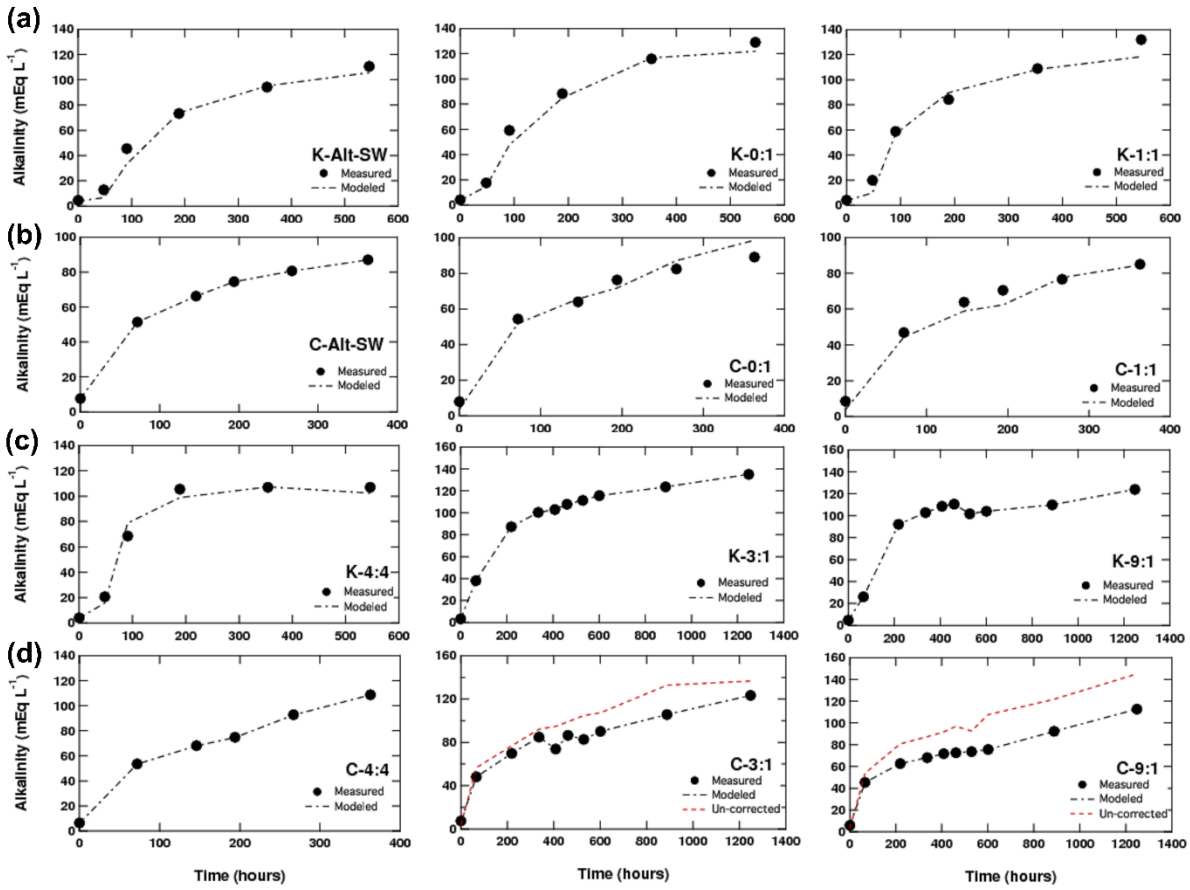

Figure 3: Comparison of experimental and modelled evolution of aqueous chemistry in samples with different seeding materials. A large discrepancy was observed in samples with kaolinite seeds (a and c) compared to calcite seeds (b and d). An increase in the mismatch between experimental and modelled results is observed with an increasing Mg/Ca. Uncorrected line indicates the initial modelled values without any addition or removal of $NaHCO_3$ from the solution input.

3.3 *Results from mineralogical characterization*

352 *Table 2: Summary of XRD results with Rietveld quantitative analysis of minerals (wt % with*
353 *estimated standard deviation) for all experiments. Calcite and Magnesium Calcite differ in*
354 *their concentration of magnesium and have different XRD patterns.*
355

Experiment – Mg:Ca	Mg/Ca	Kaolinite (wt %)	Calcite (wt %)	Magnesium calcite (wt %)	Monohydrocalcite (wt %)
K-0:1	0	87.4 ± 0.4	12.6 ± 0.4	-	-
C-0:1	0	-	100.0 ± 2.6	-	-
K-0:2	0	72.7 ± 2.9	27.3 ± 1.3	-	-
C-0:2	0	-	100.0 ± 2.0	-	-
K-1:1	1	86.7± 3.4	12.7 ± 1.3	-	-
C-1:1	1	-	87.2 ± 2.2	12.6 ± 1.1	-
K-2:2	1	84.6 ± 1.8	-	15.4 ± 0.7	-
C-2:2	1	-	85.2 ± 1.7	14.8 ± 1.7	-
K-3:3	1	80.5 ± 1.6	-	19.6 ± 0.7	-
C-3:3	1	-	55.6 ± 2.4	44.3 ± 2.2	-
K-4:4	1	66.1 ± 1.6	-	33.8 ± 1.0	-
C-4:4	1	-	44.6 ± 2.7	55.5 ± 3.0	-
K-2:1	2	92.4 ± 1.4	-	2.6 ± 1.2	5.0 ± 0.8
C-2:1	2	-	88.9 ± 2.2	11.1 ± 2.2	-
K-3:1	3	90.3 ± 1.2	-	-	9.7 ± 1.0
C-3:1*	3	-	76.0 ± 2.0	21.0 ± 1.6	3.0 ± 0.6
K-4:1	4	85.5 ± 1.0	-	-	14.5 ± 1.0
C-4:1	4	-	93.4 ± 0.7	-	6.6 ± 0.7
K-Atl-SW	5.2	87.5 ± 1.0	-	-	12.5 ± 1.0
C-Atl-SW	5.2	-	87.7 ± 2.3	4.0 ± 0.8	8.2 ± 0.5
K-9:1	9	87.6 ± 0.9	-	-	9.5 ± 0.8
C-9:1	9	-	86.1 ± 1.1	-	13.9 ± 1.0

356
357 * Average of two samples.
358

Characterization of the solid samples using XRD showed that two calcium carbonate polymorphs precipitated from all experiments: MHC and calcite (Table 2). Our experiments suggest that all solutions with Mg/Ca ratio of greater than 3 dominantly yields MHC, whereas the media with an initial Mg/Ca of 1 or less produces calcite (Table 2). The diffraction patterns for MHC and calcite align closely with the crystallographic information for $Mg_{0.1}Ca_{0.9}CO_3$ (Althoff, 1977) (Figure 4). The calcite peak becomes broader and shifts towards higher 2θ over time and with increasing magnesium concentration in the medium (Figure 4b). This peak shift and broadening indicates the incorporation of Mg into the lattice of calcite, decreasing the size of the unit cell and the crystal domains (Lenders et al., 2012; Nielsen et al., 2016; Blue et al., 2017). We observe that the mineralogy of the polymorphs precipitated is weakly affected by the type of seeding material.

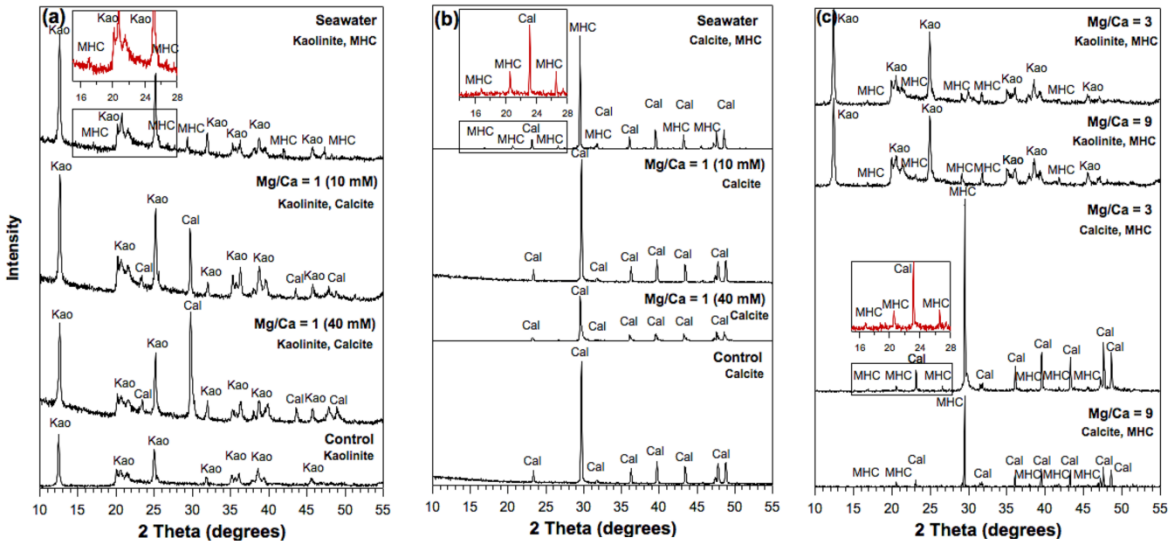

Figure 4: Powder X-Ray diffraction patterns collected from selected incubation samples in the three biotic experiments, (a) Mg/Ca=1 (kaolinite); (b) Mg/Ca=1 (calcite); and (c) Mg/Ca=3 and 9 (kaolinite and calcite). Intensity is reported in counts.

3.4 Microbial evidence in precipitate minerals

Together, solution data from our experiments show that microbial sulfate reduction alters the chemical state of the experiments with respect to calcium carbonate mineral stability. The sulfate reducing bacteria, through their metabolism, produce extremely high saturation state for all calcium carbonate polymorphs, which triggers nucleation in the presence of multiple inhibitors to nucleation and growth. The SEM images of the carbonate minerals

precipitated suggest that the sulfate reducing bacteria create a highly supersaturated micro-environment driving carbonate precipitation. We suspect that the negatively charged cell surface of the sulfate reducing bacteria initially attracts dissolved divalent cations such as calcium and magnesium (Qiu et al., 2017); in the SEM images we observe spherulitic MHC with a hollow core where clumps of well-preserved bacterial cells are located (Figure 5a and b). During carbonate precipitation, outward growth of crystals from a substrate eventually introduces geometrical competition where crystals growing normal to the substrate dominate over other orientations; this typically results in outward radiating crystal fabrics which may sometimes adopt a spherical structure if they are grown on a rounded or spherical substrate (i.e., aggregate of bacterial cells) (Dickson, 1993). Analogous observations of fossilized bacterial clump in the core of spherulitic carbonates were also found in field samples reported in Chafetz et al., (2018). In addition to the spherical MHC found, a dumbbell-shaped structure with microbial imprints was also identified in our experiments (Figure 5c and d).

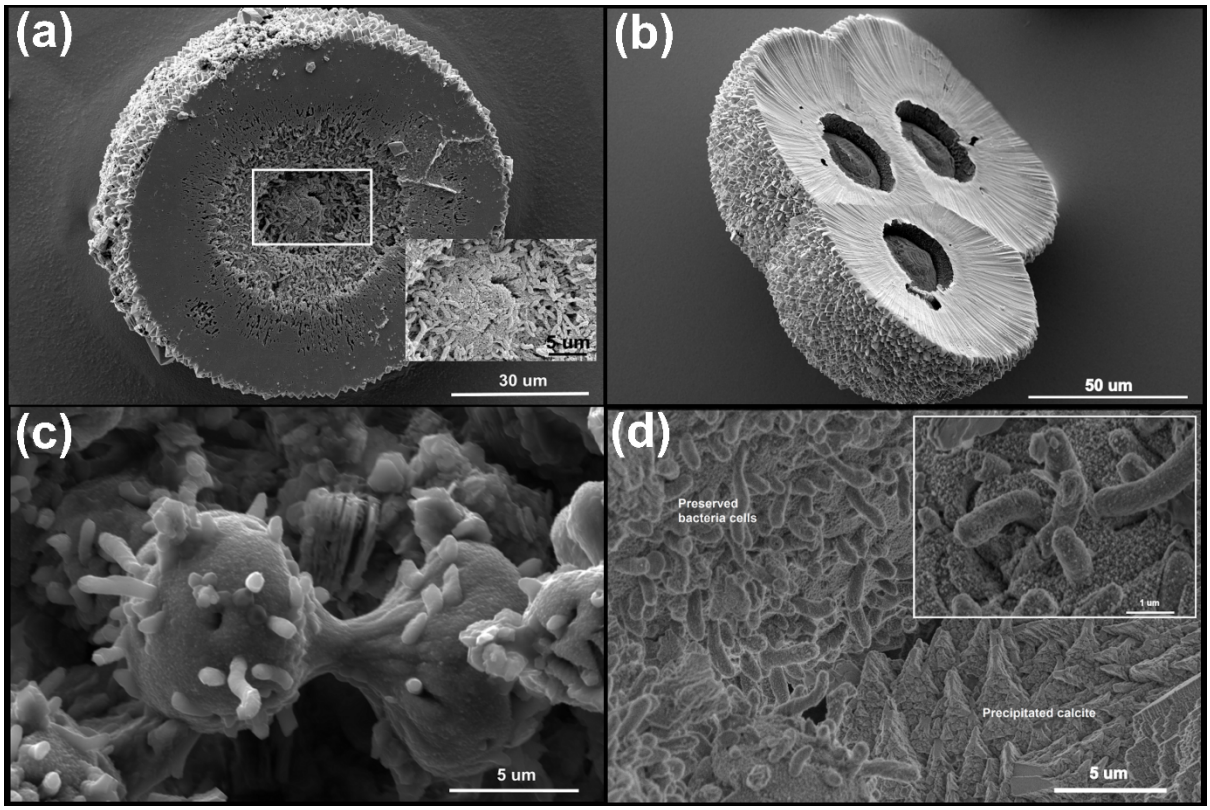

Figure 5: Evidence of microbially influenced precipitation of calcium carbonate in biotic experiments under a scanning electron microscope. SEM images (backscattered electron) showing (a) MHC hemisphere with bacteria colony concentrated at the hollow core – sample

C-Alt-SW; (b) triplet hemi-spherulitic MHC structure with hollow core – sample C-Alt-SW; (c) dumbbell-shaped structure with protruding well-preserved bacterial cell observed in sample K-4:4; (d) precipitated calcite located adjacent to fossilized bacterial colony – sample K-4:4 with closeup secondary electron (SE) image showing instantaneous calcification of Desulfovibrio bizertensis by the nano-sized crystals. All the images showing the morphology and microstructure of carbonate minerals linked to microbial sulfate reduction.

3.5 *Transformation experiment*

Four different media combinations were tested to examine which stable calcium carbonate polymorphs form from the MHC produced during our experiments (Table 3). For this, pure, spherulitic MHC was used (with diameter range between 20 – 40 µm) which had been previously precipitated from an unseeded incubation (Figure 6a). Note the distinct size and morphological difference between the biotic and abiotic precipitated MHC (Figure 6a and b). In pure seawater, this MHC transforms into both calcite and aragonite (Table 3). In this case, the dehydration of MHC changes its spherulitic structure to elongated needle-like calcite and aragonite crystals (Figure 6c). Incubation of MHC with pure MQ-water transforms the MHC into calcite (Figure 6d). In contrast, when the transformation happens in seawater with yeast extract or inorganic phosphate, a considerable amount of MHC is retained and not transformed into a more stable calcium carbonate polymorph (sample T-Alt-SW-YE - 79.5 ± 1.5 %, sample T-Alt-SW-PO4 - 26.2 ± 1.7%) (Figure 6e and f). One possible explanation for the stabilization of MHC in medium with phosphorus enriched solution is the common ion effect.

Table 3: Mineralogical composition of calcium carbonate polymorphs (in wt %) derived from MHC transformation.

Medium	MHC	Calcite	Mg-Calcite	Aragonite
T-Atl-SW (Seawater only)	-	77.1 ± 3.9	-	22.9 ± 3.9
T-MQ (MQ-water only)	-	100.0 ± 0	-	-
T-Atl-SW-YE (Seawater + yeast extract)	79.5 ± 1.5	15.5 ± 1.2	5.1 ± 1.2	-
T-Atl-SW-PO4 (Seawater + K_2HPO_4)	26.2 ± 1.7	52.3 ± 3.1	-	17.2 ± 1.3

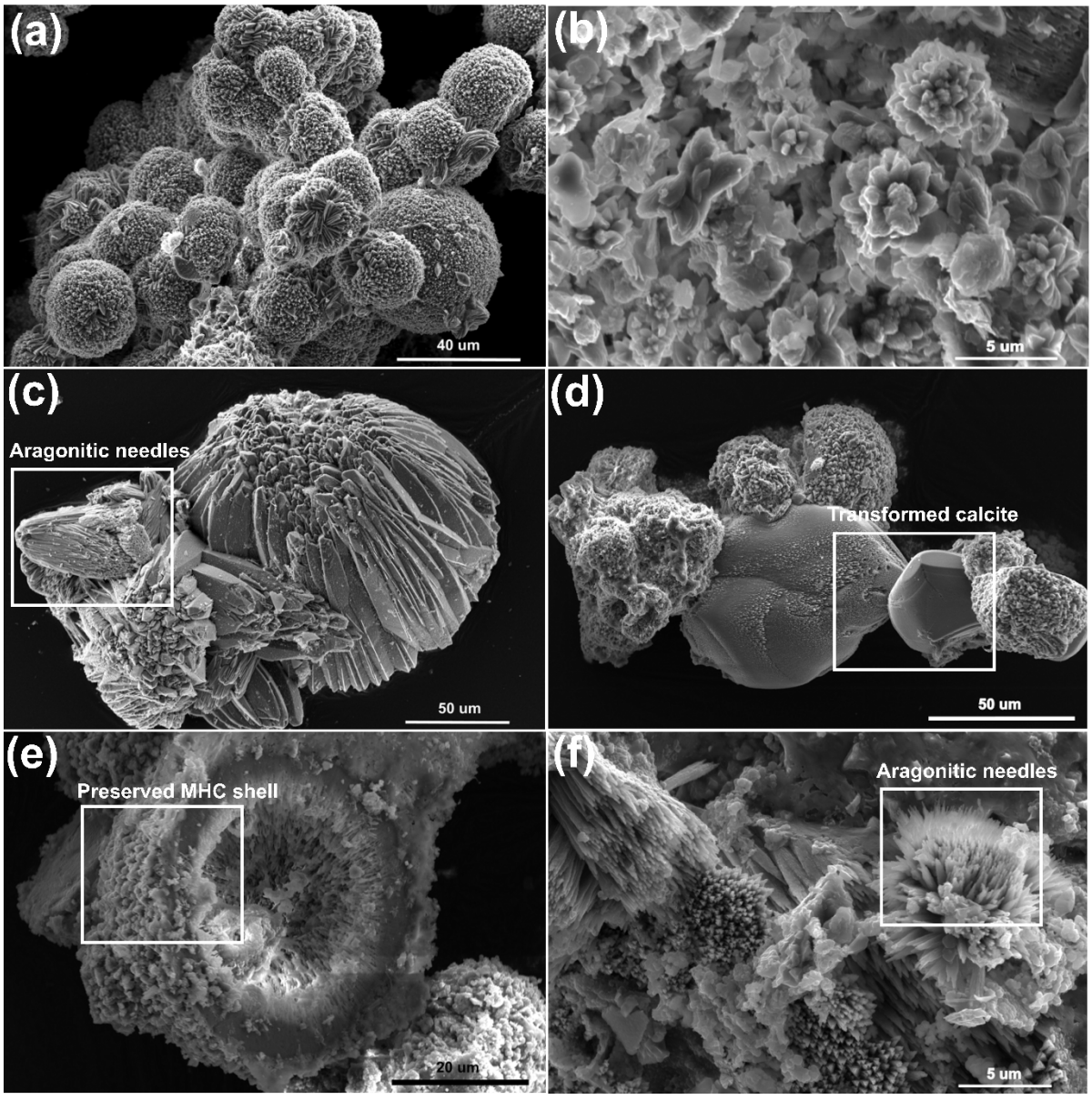

Figure 6: SEM images show the morphology of minerals precipitated in the biotic and abiotic experiments. (a) Initial spherulitic MHC from the biotic experiments; and (b) sub-micron aggregated platelets (cauliflower-shaped) MHC from abiotic experiment. The mineralogy of

these final products was confirmed using XRD. Image (c) – T-Alt-SW, (d) – T-MQ, (e) – T-Alt-SW-YE, and (f) – T-Alt-SW-PO4 are transformation products of 5a after thermal dehydration at 100˚C for 48 hours. We note the distinct morphological alteration of the final products (aragonitic needles, calcite rhomb and bigger hollow core of preserved spherulitic MHC). Mineral composition of these final polymorphs is reported in Table 3.

4.0 DISCUSSION

Our results indicate that microbial sulfate reduction triggers the precipitation of calcite and MHC. Which of these may dominate appears to depend on the Mg/Ca ratio at the time of mineral nucleation; MHC forms from solutions with Mg/Ca greater than 3, while calcite forms from solution where the Mg/Ca ratio is 1 or less. Our media is initially undersaturated with respect to all carbonate minerals, but within 100 hours the media is super saturated and precipitation of calcium carbonate occurs. The rate of precipitation depends on the calcium concentration in the media, and ironically the mineral seed present, and is independent of the Mg/Ca ratio.

The discussion is divided into five parts. First, we discuss the influence of microbial sulfate reduction on the evolving solution chemistry driving carbonate mineral precipitation. Then we discuss the primary controls on the formation of MHC and calcite in these experiments. Next, we demonstrate the effect of seeding materials on the solution chemistry and also the calcium carbonate polymorphs precipitated. In the penultimate section of the discussion, we show the controls on the transformation of MHC to more stable polymorphs. Finally, we explore the implications of our results on sedimentary carbonate precipitation in the natural environment.

4.1 The influence of microbial sulfate reduction on calcium carbonate precipitation

Our experimental results show that microbial sulfate reduction strongly influences solution chemistry and thus, affects carbonate mineral precipitation in three ways. First, each

experiment is accompanied by a significant increase in total alkalinity and pH as microbial sulfate reduction proceeds (Figures 1d, 2d) through the overall reaction (Gallagher, 2012):

$$4CHO_2^- + SO_4^{2-} + H_2O \rightarrow 4HCO_3^- + HS^- + OH^- \quad \text{(Eq. 1)}$$

This relationship suggests an increase of one mole of dissolved inorganic carbon (DIC) as well as an increase of 1.2 moles of total alkalinity per mole of organic carbon oxidized (Soetaert et al. 2007). This increase in alkalinity leads to dramatic increases in the carbonate mineral saturation state. For example, within the first 100 hours of experiments with kaolinite seeds, we see a 10 to 15-fold increase in alkalinity, which translates to calcite saturation index of ~1 - 2 ($SI_{Calcite}$). After carbonate mineral growth begins, the continued increase in pH and DIC from the growth of the sulfate reducing bacteria is matched by a decrease or stabilization of the pH and DIC concentration due to calcium carbonate precipitation.

This increase in alkalinity from microbial sulfate reduction coupled to formate oxidation was closely replicated with PHREEQC modeling for the experiments with the kaolinite seeds (Figure 3). We did, however, note several mismatches in the PHREEQC modeling of our experiments with calcite seeds, in that the modeled alkalinity was higher than the measured alkalinity. We suspect there is a sink for alkalinity in the experiments with calcite seeds that does not exist with the kaolinite seeds. One possibility is the secretion of exopolymeric substances (EPS) by the sulfate reducing bacteria, which can complex cations across a wide range of solution pH (Braissant et al., 2007; Dupraz et al., 2009; Baker et al., 2010). EPS was not included in the PHREEQC model, due to the complexity of chemical reactions and the different structural forms of EPS and we suspect that this might account for the mismatch between the modelled and measured alkalinity.It is unclear why the sulfate reducing bacteria might make more EPS in the experiments with calcite seeds, although this was observed in three separate experimental runs and thus the result is reproducible. In addition, the adsorption onto and desorption from the mineral seeds' surfaces, and the exchange of CO_2 with the headspace might account for alkalinity difference that we could not estimate and include in the model. Despite the mismatch in some of the calcite seeding samples, we were able to model most of the samples with good agreement between the measured and modelled alkalinity (figure 3).

Although Soetaert et al. (2007) suggested that microbial sulfate reduction alone may not lead to carbonate mineral precipitation because the solution pH is poised too low (the equivalence midpoint is pH 6.7), recent modelling and culture experiments support the notion that microbial sulfate reduction may lead to carbonate mineral precipitation. For example, Meister et al. (2013) demonstrated that while microbial sulfate reduction initially lowers pH, the carbonate saturation state decreases at first but slowly increases as sulfate reduction continues due to increasing dissolved inorganic carbon concentration while pH stabilizes. The Meister et al (2013) results are in agreement with our observations – that the chemical evolution of closed (or diffusionally controlled) systems is strongly dependent on the amount of organic carbon respired, and therefore dissolved inorganic carbon generated, in addition to other variables such as pH and buffering capacity.

Second, aside from increases in dissolved inorganic carbon and carbonate saturation state, the concentration of inhibitors of carbonate mineral precipitation, such as sulfate and magnesium, changes over the course of our experiments (Walter and Burton, 1986; Burton and Walter, 1989; Grases and March, 1990; Lin and Singer, 2005). Although sulfate has long been understood to inhibit calcite precipitation (Busenberg and Plummer, 1985; Walter, 1986 Bots et al., 2011), especially in the presence of elevated concentrations of aqueous magnesium (Bots et al., 2011; Nielsen et al., 2016), our results show that calcium carbonate mineral nucleation occurs as sulfate is being depleted, but while there is still substantial aqueous sulfate in solution. Furthermore, the Mg/Ca ratio in our solution increases over the course of the experiments. Because the Mg/Ca ratio is recognized as a fundamental control on calcium carbonate polymorphism, changes in this parameter should influence the final carbonate mineral products.

It is interesting to note that the spherulitic structure of carbonate minerals is not unique to microbial sulfate reduction. Rather, variables such as Mg/Ca ratio (between 2 to 8), salinity, and precipitation rates collectively control the habit and structural form of the carbonate precipitated (Tracy et al., 1998; Sanchez-Navas et al., 2009). Spherulitic growth is also a common product resulting from crystallization of ACC. Spherulitic growth requires a large

crystallization driving force, such as a solution with sustained supersaturation from initial formation and subsequent continuous dissolution of ACC, resulting in the aggregation and growth of spherical nanoscale mineral particles (Granasy et al., 2005; Han et al., 2017a; Rodriguez-Blanco et al., 2017). Some field sedimentary characteristics of dolomite also reflect spherulitic growth processes, suggesting that the deposition and crystallization process may have involved the transformation of an amorphous precursor, and thus high supersaturation states (Hood et al., 2011). The hollow core structure of the spherulitic MHC with calcified microbes texture in our experiments are not visible in precipitation products of abiotic precipitation experiments (Bots et al., 2012; Rodriguez-Blanco et al., 2014), hence, could serve as unique signature of microbial mediated precipitation that holds considerable interests for most sedimentary geologists. However, our transformation experiments suggest that such a structure and the associated microbial texture are difficult to preserve and could be vulnerable to post-burial processes and diagenesis (e.g. remineralization).

We suspect our carbonate mineral products must have initially transformed from an amorphous phase (ACC) prior to crystallization into calcite or MHC. The amorphous phase is often found present together with some other crystalline sample with Bragg peaks on the XRD pattern. Visual examination under SEM also indicates that both amorphous and crystalline solid phase coexist during the early stage of the precipitation (Supplementary Materials H). Furthermore, as we discuss below, saturation state and calcium carbonate mineralogy provide additional evidence for the role of an amorphous calcium carbonate precursor. Depending on the Mg/Ca ratio of the surrounding fluid, the ACC and calcite may incorporate different amounts of water into the structure due to the difference in hydration energy between the magnesium and calcium ions (Christ and Hostetle, 1970; Gonzalez, 2009; Tommaso and de Leeuw, 2010; Hopkinson et al., 2012; de Choudens-Sanchez and Xu et al., 2013; Nishiyama et al., 2013; Sun et al., 2015). Such a difference in hydration energy has also been shown to affect the transformation into crystalline calcium carbonate polymorphs and induce the transformation of ACC to MHC rather than calcite (Rodriguez-Blanco et al., 2014). The structure of calcite precipitated in the experiments with lower Mg/Ca forms rhombohedral shapes with triangular terminations (Figure 6d).

4.2 Evolving chemical controls on $CaCO_3$ precipitation and polymorph selection

The chemical evolution discussed above establishes a framework for interpreting the mineral products formed in our experiments, and for predicting the calcium carbonate mineral phases that may be associated with microbial sulfate reduction more broadly in the natural environment. An unexpected observation from our experiments is the dominance of monohydrocalcite in the biomineralization products, a relatively rare calcium carbonate polymorph in natural systems. Previous work suggests that at Mg/Ca ratios of greater than ~2, aragonite nucleation dominates calcium carbonate mineral precipitation, and therefore the carbonate mineral products precipitated from modern seawater (Katz, 1973; Berner, 1975; Burton, 1993, Ries et al., 2008; Bots et al., 2011). However, aragonite is conspicuously absent in all of our experiments (and, indeed, in nearly all microbially induced carbonate precipitation experiments) despite initial Mg/Ca ratios that ranged from 0 – 9 (Table 2). This indicates a strong inhibition of aragonite nucleation in our experiments, remembering that aragonite has a higher energy barrier to nucleation compared to other polymorphs such as MHC, which we suspect results from elevated phosphate concentrations. Previous studies have shown that a phosphate concentration of greater than 10 µM inhibits the formation of aragonite, and even phosphate concentrations as low as 5 µM can alter the kinetics of aragonite precipitation (Walter, 1986; Oomori et al., 1988; Burton and Walter, 1990; Yagi and Fukushi, 2011; Tadier et al., 2017). The phosphate concentration in our experiments ranged between 600 – 800 µM, which is an order of magnitude higher than seawater and on the higher range of that measured in anoxic sediments (Sasaki et al., 2001; Hyacinthe and Van Cappellen, 2004; Sinkko et al., 2013; Egger et al., 2015; Kipp and Stueken, 2017). However, we suspect that the range of phosphate concentrations in our experiments does not affect the types of final polymorphs precipitated and inhibits the formation of aragonite, while not high enough to precipitate calcium phosphate minerals. In our MHC transformation experiments, the role of phosphate in the inhibition of aragonite is also shown as none of the experiments with added phosphate produced aragonite, in spite of high Mg/Ca; we also observed this in abiotic experiments that we include in Supplementary Materials C. Phosphate adsorbs rapidly and irreversibly on high energy sites (kink, step, edge and hole) of mineral surfaces, which drives the inhibitory effects on carbonate mineral growth and dissolution rates (Berner and Morse, 1974).

One possible consequence of the presence of phosphate in our experiments is that the saturation state for various calcium carbonate polymorphs increases well beyond typical range needed for aragonite or calcite nucleation from seawater (Morse and He, 1993). In our experiments, we do not observe calcium carbonate nucleation until the ionic activity product is well above that required for initial ACC precipitation (Figures 1g). These solution data hint that, in the absence of aragonite and calcite nucleation, ACC is the solubility-limiting phase in our experiments, providing a reactive and transient precursor to the formation of more stable crystalline calcium carbonate mineral phases.

In addition to the exceptionally high saturation states needed for carbonate mineral precipitation, the likely initial formation of ACC in our experiments provides a simple mechanism to explain observed carbonate polymorphism. Previous studies have shown that once formed, ACC transforms to several carbonate polymorphs depending on the Mg/Ca, pH, and concentration of DIC (Loste et al., 2003; Kimura and Koga, 2011, Nishiyama et al., 2013; Rodriguez-Blanco et al., 2014; Blue et al., 2017). In particular, at high Mg/Ca (above 8, depending weakly on pH and concentration of dissolved inorganic carbon) ACC has been shown to transform to MHC.

Our results suggest that microbial induced ACC transforms to MHC at much lower Mg/Ca than previously shown in these abiotic experiments (Rodriguez-Blanco et al., 2014; Blue et al., 2017). Our results are superimposed on the stability fields for MHC initially proposed by Blue et al. (2017) (Figure 7). We show that dominant carbonate mineral polymorph is determined by the solution chemistry at the time of carbonate mineral nucleation, and although the solution chemistry then evolves into other stability fields (Supplementary Material I), the initially precipitated polymorph continues to grow. Our experiments suggest a shift in the calcite-MHC boundary to a $a\mathrm{Mg}^{2+}/a\mathrm{Ca}^{2+}$ of 2. However, the abiotic experiment in Blue et al. (2017) did not have phosphate which we already suspect has influenced carbonate mineralization pathways. Therefore, the apparent stability field suggested by this study may be partly due to the role of phosphate.

These experimental results suggest that the experiments where MHC precipitates (higher Mg/Ca ratios) have a longer delay prior to initial mineral precipitation, and a lower pH drop

compared to the experiments that precipitate calcite. This may be due to the incorporation of magnesium in the initial ACC, which has been suggested to stabilize ACC and retard the time required for transformation (Lin et al., 2015; Purgstaller et al., 2017). In addition, magnesium incorporation likely decreases the effective solubility of both the ACC and MHC polymorphs, although this is not quantitatively understood at present (Fukushi et al., 2017; Purgstaller et al., 2017).

The evolution of solution chemistry and the formation of different calcium carbonate polymorphs here are comparable to other experiments involving carbonate mineral precipitation and microbial populations conducted by Balci et al. (2016) and Han et al. (2017). Both studies investigated the role of halophilic bacteria in the precipitation of carbonate minerals. Dypingite, hydromagnesite, aragonite, MHC, huntite and struvite were the primary carbonate minerals that precipitated from a hypersaline solution (Balci et al., 2016; Arias et al., 2017) whereas Han et al., (2017) found MHC, calcite and Mg-rich calcite in varying sodium chloride solutions (3 – 20% w/v) cultured with *Chromohalobacter Israelensis*. In contrast to culture experiments reported by Rivadaneyra et al., (1998; 2010), our culture samples with high (Mg/Ca = 3) did not precipitate any aragonite. This is probably due to the fact that Rivadaneyra et al., (1998; 2010) incubated their samples at a higher temperature (32˚C) and liquid-limited environment (a glass coverslip) – however the presence of water molecules (or activity of water) is the key for hydrated phase MHC to form.

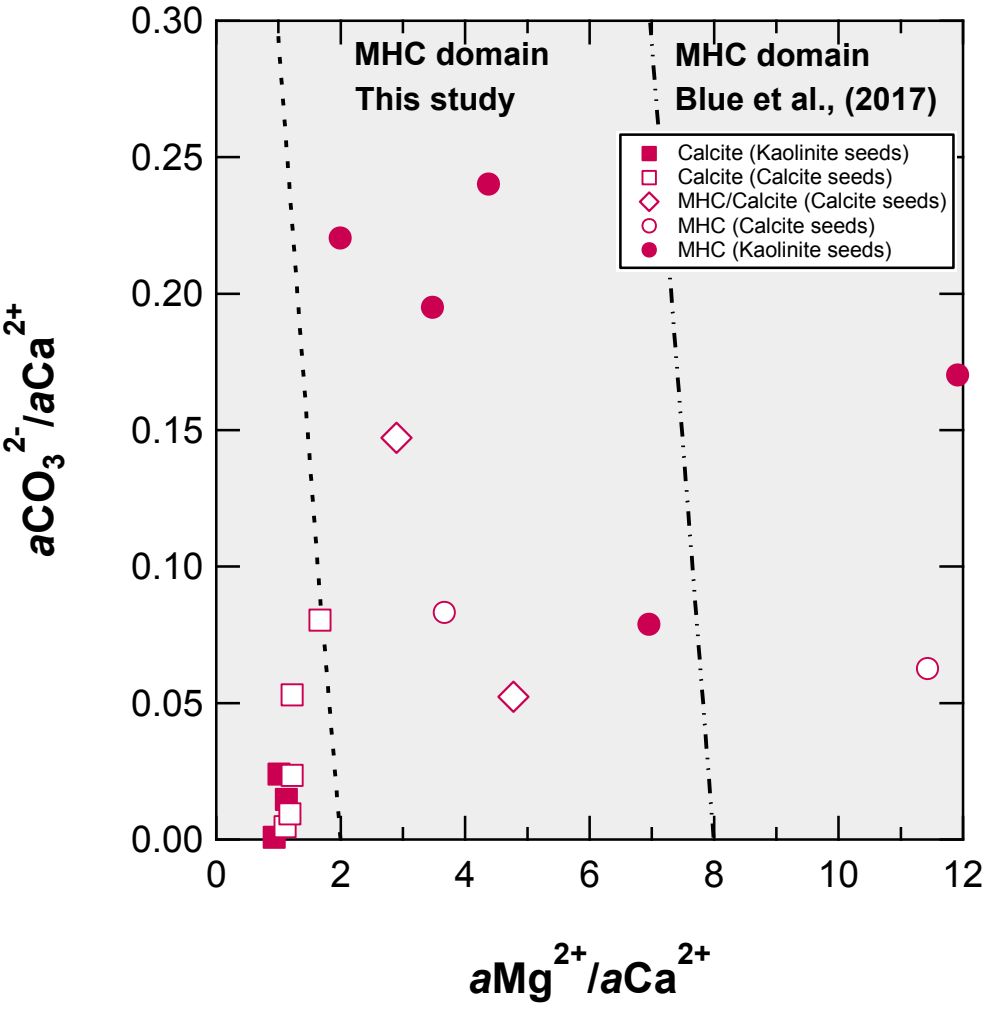

643 *Figure 7: Samples with different Mg/Ca prior to precipitation of calcium carbonate (nucleation stage) were plot against* aCO_3^{2-}/aCa^{2+} to show the stability field for MHC and calcite.. *Square symbols indicate calcite is the final polymorph while circle symbols indicate MHC as the major stable product at the end of the incubation experiment. Diamond symbols indicate solid samples with mix mineralogy (both MHC and Mg-calcite), where MHC dominates. Open symbols marked samples with calcite as seeding material while close symbols are kaolinite seeded samples. The experiments from this study were plotted on an abiotic stability field delineated Blue et al., (2017). Note the boundary of MHC domain has shifted towards left (from* aMg^{2+}/aCa^{2+} *approximately 2 to 8) in the microbial induced studies, suggesting the effect of phosphate in stabilizing the MHC in biotic studies.*

654

655 In addition to promoting non-traditional calcium carbonate mineralisation pathways in our
656 experiments, high phosphate concentrations might also explain the exceptional stability of
657 MHC in our incubation and transformation experiments. In a phosphate-free solution, any

MHC we formed through microbial induction should have transformed into a more stable carbonate polymorph over time, even at room temperature. However, the precipitated MHC in our experiments did not transform after sitting in the lab over a year with the old media, suggesting something inhibits MHC transformation (Supplementary Material J). Furthermore, the mass basis sorption capacity of MHC is significantly higher than those of aragonite and calcite, which may explain the greater impact of phosphate in stabilizing MHC (Yagi and Fukushi, 2011; Fukushi et al., 2011). It is also possible that the formation of much stable calcite/calcium phosphate around the outer shell shields the inner MHC from transforming by protecting the interior of the spherulitic MHC from exposure to the medium. Besides the role of phosphate on MHC stabilization, previous studies done by (Omoike and Chorover, 2006; Steiner et al., 2010; Gallagher et al., 2013) also pointed out the possible role of organic acids such as carboxylic acids and EPS in stabilizing the precipitated minerals, where it is thought that the EPS could adsorb or to be entrained within the mineral and significantly reduce its reactivity.

4.3 Influence of seeding material on the formation of calcium carbonate polymorphs

Microbially-induced carbonate mineral precipitation and polymorphism also appears to depend on the mineral seeds that are present. Overall, MHC tends to dominate products from experiments with kaolinite seeds compared to those conducted with calcite seeds (Table 2 and Figure 8). In addition, MHC forms at slightly lower Mg/Ca ratios in the experiments with kaolinite seeds compared to calcite seeds. We suspect that the delayed and muted precipitation of MHC in calcite-seeded experiments results from initial overgrowth of a higher-magnesium calcite phase on the calcite seeds. Growth of calcite on calcite seeds require a lower supersaturation for nucleation and growth to initiate, thereby lower the induction time and pH for nucleation to happen. A similar observation has been reported in Lioliou et al. (2007) showing that the types of seeding materials can impact precipitation kinetics. SEM images (Figure 9) illustrate an epitaxial growth relationship between the original calcite seeds and precipitated calcite, which ranges from submicron to nano-sized. A similar observation was also reported in Rodriguez-Navarro et al. (2012) where they found that there is an overruling factor of substrate types on the mineralogy of calcium carbonate precipitated. In these experiments, where calcite overgrowth forms, MHC is never observed, and conversely, where there is no calcite overgrowth, MHC is

precipitated. There are two exceptions to this: the C-3:1 and C-Alt-SW experiments generate products of mixed mineralogy which could result from multiple precipitation events over the course of the experiment as the Mg/Ca ratio is evolving. No apparent drops in pH or alkalinity were observed in the samples with overgrowth on calcite seeds, suggesting the buffering effects from the calcite seeds impedes high pH values (particularly CO_3^{2-}/Ca^{2+}) in the system, and therefore, MHC is not favoured. Such a difference in precipitation kinetics in experiments with different seeding materials is illustrated in the change of calcium concentration. Nearly all experiments with calcite seeds (except the experiments where we get mixed mineralogy in the final solid products) showed a gradual decrease of calcium concentration while the calcium concentrations drop rapidly in experiments where kaolinite is used. Particularly in the calcite-seeded experiment, we note a trivial drop in calcium concentration prior to the main precipitation event, suggesting slight removal of calcium during the nucleation process (or epitaxial growth on calcite seeds) before main mineral precipitation follows. Homogeneous precipitation is more likely to occur in the kaolinite-seeded experiments where there is less buffering capacity in the supersaturated solution. Such a sample is often characterized by a sharp drop in pH and calcium concentration (e.g. K-9:1).

Intriguingly, these results suggest that MHC is only present at Mg/Ca ratio of 3 in the calcite-seeded experiments; while MHC is dominant at Mg/Ca ratio of 2 in the kaolinite-seeded experiments (Figure 8). Calcite seeds show an increase in the amount of MHC precipitated as the Mg/Ca ratio increases, whereas the amount of MHC precipitated peaks at Mg/Ca = 4 and drop at Mg/Ca > 4 in experiments with kaolinite seeds. We also note that there is less consistency in the carbonate mineral polymorphs precipitated between replicates of calcite-seeded experiments. Such ambiguity is not observed in kaolinite seeded experiment, where the boundary of calcite/MHC domain is more clearly defined at a Mg/Ca ratio of 2.

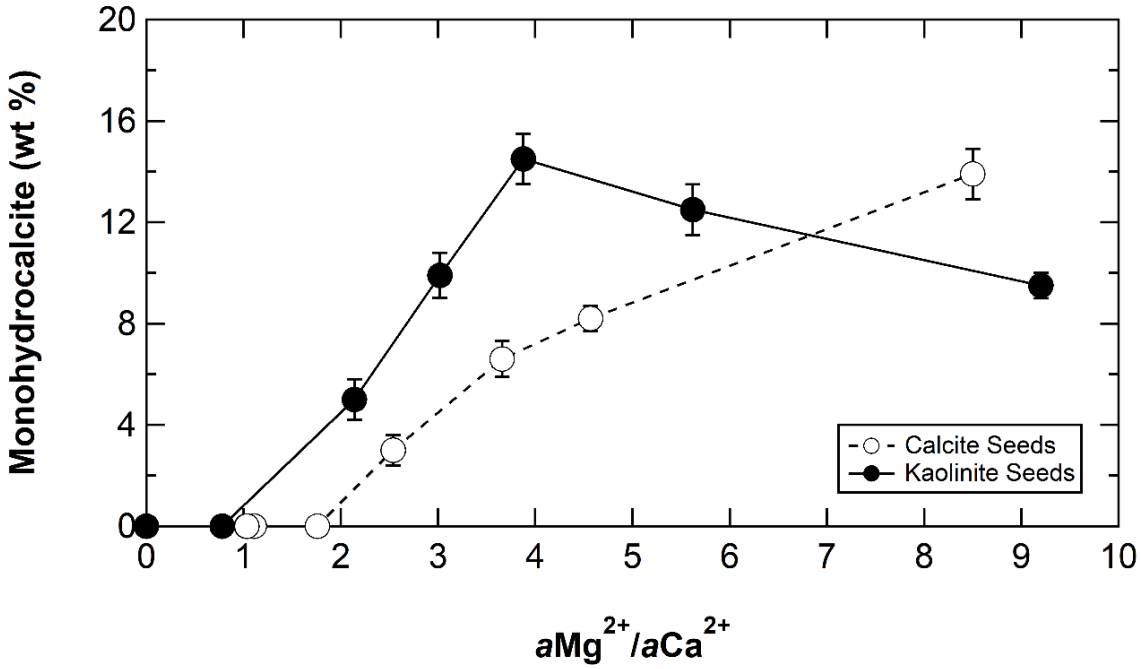

716

717 *Figure 8: The precipitation of MHC in wt % (of total solid sample) as a function of Mg/Ca*
718 *(before precipitation) in experiment with different seeding materials. Error bars represent*
719 *the estimated standard deviation calculated from Rietveld refinement.*

720

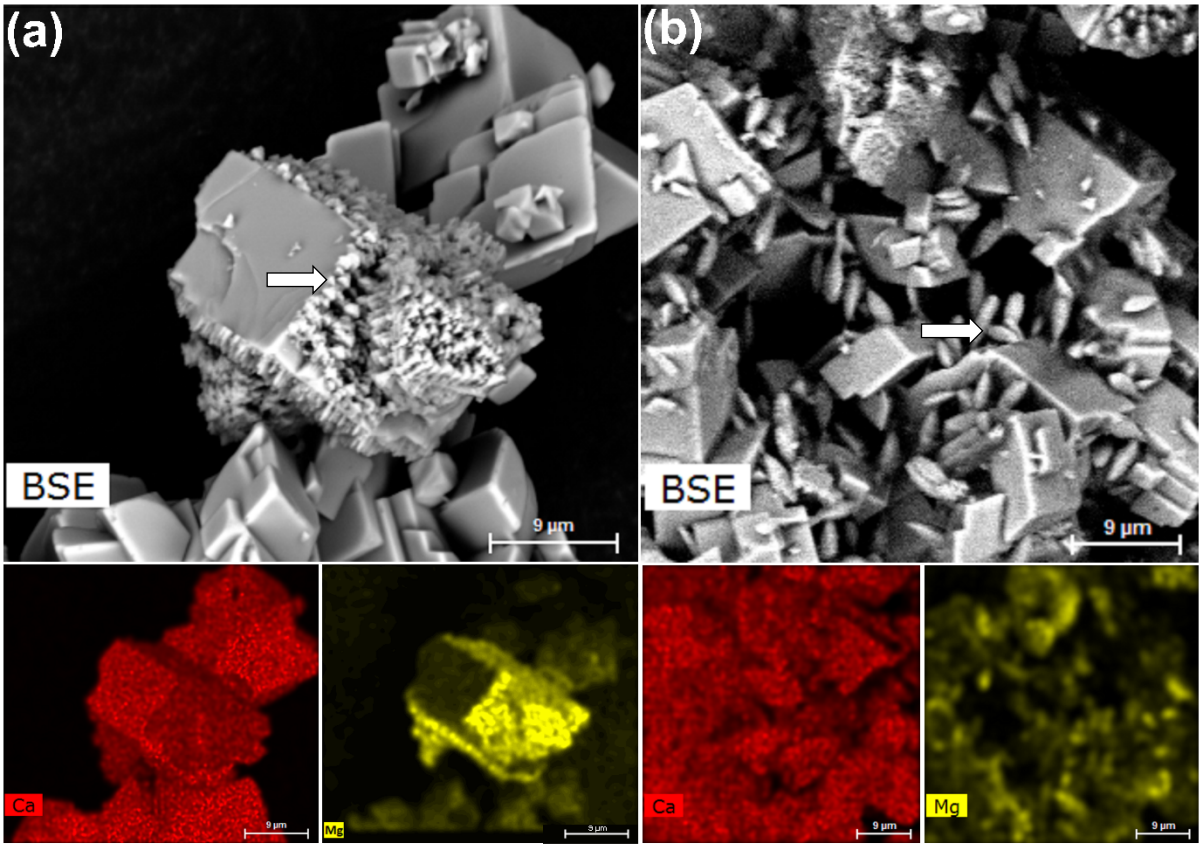

721
722 *Figure 9: Submicron to nano-sized magnesium calcite crystals grow on calcite seeds (a) C-3:1*

723 *and; (b) C-2:1. Arrows show two forms of magnesium calcite growing epitaxially on calcite*
724 *seeds.*
725
726 ***4.4 Synthesis, stability and transformation of MHC***
727 The earliest studies of MHC formation suggest that three conditions had to be met for MHC
728 to form: (1) the Mg/Ca ratio must be high; (2) the water temperature should be < 40 ˚C; (3)
729 The water should be oversaturated with respect to calcite, aragonite, and MHC, while
730 preventing oversaturation with respect to hydroxy- and fluorapatite (Stoffers and Fischbeck,
731 1974; Oomori et al., 1988). Our results are consistent with these geochemical conditions.
732 Regardless of the seeding material used, we found that SI_{MHC} has to be greater than one for
733 MHC to form (Figure 10). Mixed mineralogy of MHC and calcite (often higher in MHC) is
734 particularly observed at a lower Mg/Ca ratio (between 2 to 4), whereas we found that only
735 MHC precipitate as the Mg/Ca increases. Our results also agree with findings reported by
736 Rodriguez-Blanco et al. (2014) in a series of abiotic experiments where MHC is absence at
737 Mg/Ca lower than two although the solution is highly supersaturated with respect to MHC
738 (SI_{MHC} = 2). However, in their experiments, MHC precipitates when the solution SI_{MHC}
739 approached 2.5 or higher, suggesting that the supersaturated solution alters the
740 precipitation kinetics to favor the formation of MHC. Such a high saturation condition,
741 however, rarely occurs in biotic studies or in the natural environment.
742
743 Contrary to previous work that suggests that it is magnesium that stabilizes MHC, we
744 suggest that phosphate plays a larger role based on abiotic experiments (Supplementary
745 Materials C) and electron backscatter mapping of our samples (Figure 10a and b) (Dejehet et
746 al., 1999). These images indicate that the outer shell of MHC before (Figure 11a and b) and
747 after (Figure 11c and d) the mineralogical transformation is relatively low in magnesium but
748 enriched with phosphorus (Figure 11a, b, c and d). Higher magnesium concentrations were
749 found in the inner shell, suggesting the inner shell is initially composed of more Mg-rich
750 carbonate phases (Figure 11b and c). We suspect that the inner shell could be unstable,
751 nano-crystalline, less dense and associated with the bacterial colony that formed early in
752 the nucleation stage (Supplementary Materials K). The EDS images thus imply the important
753 role of magnesium in MHC nucleation, while phosphate is linked to MHC stabilization.
754 Previous studies suggest that the stabilization of phosphate on calcite is due to

chemisorption of orthophosphate onto the most actively dissolving sites of the calcite surface (Berner and Morse, 1974; Morse 1974; De Kanel and Morse, 1978; Edmund Wajon et al., 1985). During the transformation process this unstable phase is susceptible to dehydration and deformation via nano-voids or cracks in the MHC, leaving a hollow chamber behind. Comparable features have been previously observed in studies involving other calcium carbonate polymorphs (Suzuki et al., 2006; Chen et al., 2008). Through our transformation experiment, we observe that the phosphate-rich outer layer of MHC is more stable compared to the inner core (Figure 11c), although the exact mechanism how phosphate stabilizes MHC requires further investigation.

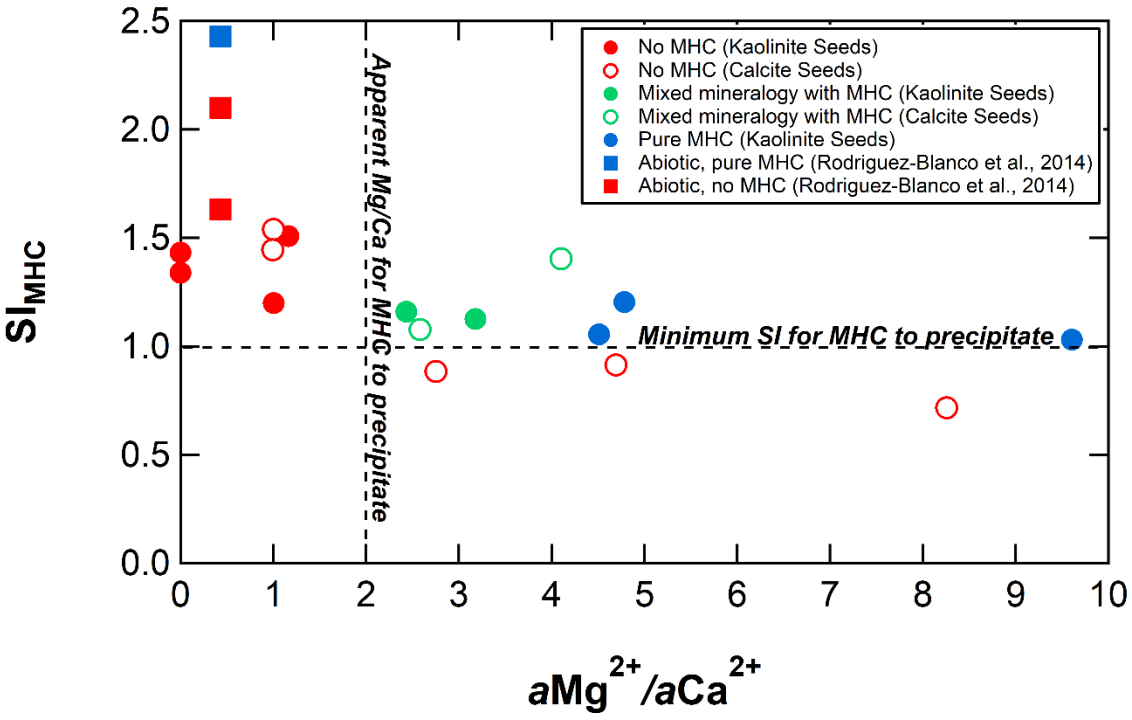

Figure 10: Cross plot between saturation index and aMg^{2+}/aCa^{2+} indicates that SI_{MHC} higher than 1.0 is required for the formation of MHC at aMg^{2+}/aCa^{2+} greater than 2. The data points are measurements taken before the precipitation of calcium carbonate. Abiotically precipitated calcium carbonate reported in Rodriguez-Blanco et al. (2014) were compared and given in square symbols.

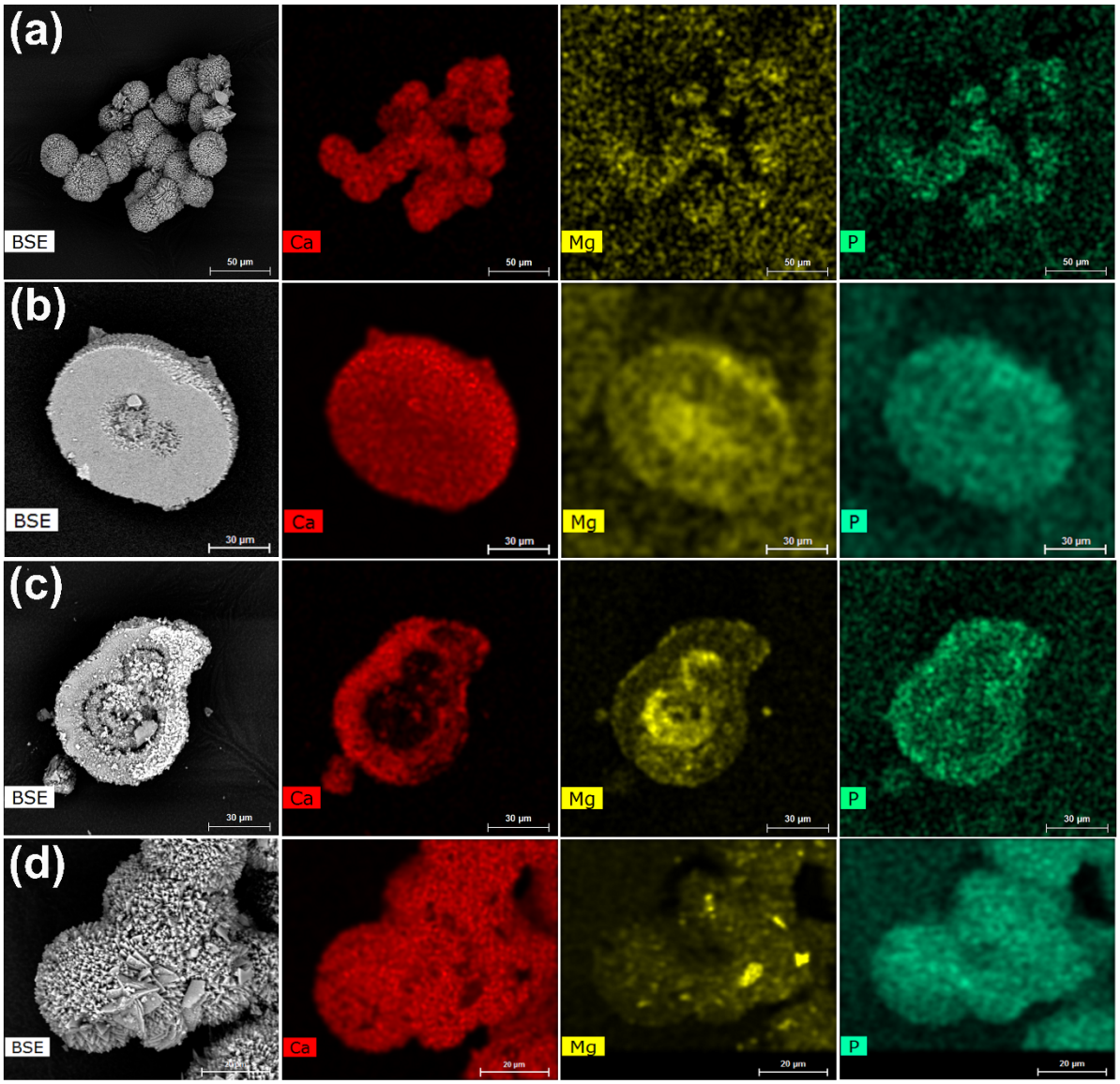

Figure 11: SEM elemental mapping (Ca, Mg and P) of MHC. (a) chemical composition of MHC prior to transformation experiment; (b) hemispherulite MHC with higher Mg distribution at the core prior to transformation; (c) cross section of spherulitic MHC (T-Atl-SW-YE); and (d) surface chemical compositions of MHC (T-Atl-SW-YE) after transformation process.

4.5 The role of microbial sulfate reduction in carbonate polymorphism in the natural environment

Even if MHC forms under the three conditions above in the natural environment, MHC should readily dehydrate and transform into more stable calcium carbonate polymorphs with time. Therefore, we suggest a fourth condition has to be met to find MHC in the natural environment: (4) phosphate and magnesium must be in solution, which we have

783 shown helps stabilize MHC. This is largely true in anoxic marine sediments which have high
784 magnesium from seawater and high phosphate from the combined effects of organic carbon
785 oxidation and the liberation of adsorbed phosphate from iron-oxide reduction (Hyacinthe
786 and Van Cappellen, 2004). To understand the presence of MHC in natural sediments, we
787 must also constrain the transformation of MHC to stable calcium carbonate polymorphs at
788 low temperatures; in this regard, our laboratory temperatures are warmer than most
789 sedimentary conditions.
790
791 In the natural environment, MHC can be formed as a transitional diagenetic phase in the
792 recrystallization process of metastable ikaite to final calcite (Dahl and Buchardt, 2006). The
793 formation of these minerals is often associated with microbial activity, organic materials and
794 the presence of algal mats such as in the sediment of Lake Kivu (Central Africa) (Stoffers and
795 Fischbeck, 1974). Authigenic MHC typically has been found in lacustrine environments, but
796 it also occurs in caves, as weathering products, and fjords (Dahl and Buchardt, 2006). These
797 MHCs are reported to vary in morphology (spherulitic or euhedral) and chemical
798 compositions (variations in magnesium content). For example, several studies have reported
799 the occurrence of spherulitic crystal aggregates in fluid characterized by high organic
800 material and the presence of microorganisms such as microbes and algae (Stoffers and
801 Fischbeck, 1974; Taylor 1975; Teller and Last, 1990; Dahl and Buchardt, 2006). We found
802 close resemblance of some of these naturally-occurring spherulitic MHC with the MHC
803 precipitated in our experiments. This suggests an extended period of supersaturation with
804 respect to MHC in the solution. Nearly all the aqueous phase sample where MHC is forming
805 shared similar geochemical conditions with what we proposed in this study – low
806 temperature, high pH, high alkalinity, high molar Mg/Ca ratios (> 3), and elevated PO_4^{3-}
807 concentration (> 10 μM).
808
809 Our results suggest strongly that microbial sulfate reduction drives calcium carbonate
810 precipitation and will influence the carbonate polymorph of the precipitated sedimentary
811 carbonate. If we apply our laboratory experiments to the natural environment, we
812 anticipate sulfate will have a lesser inhibitory effect on sedimentary carbonate formation
813 relative to dissolved phosphate and magnesium. This is partially due to the nucleation effect
814 of the sulfate reducing bacteria, which may counter the inhibition effect of dissolved

aqueous sulfate. Nevertheless, we sum the influence of the various variables influencing calcium carbonate polymorphism via microbial sulfate reduction under a closed system as follow: Mg/Ca >> PO_4^{3-} >> SO_4^{2-}. Although we have demonstrated that microbial sulfate reduction can be directly linked to the formation of MHC and other different calcium carbonate polymorphs, whether microbial sulfate reduction in the environment directly involves in the precipitation of MHC is still unclear. It should be noted that the pore-fluid where these microbes thrive in marine sediment is often characterized by the prerequisite geochemical conditions for MHC to form, such as high alkalinity and the presence of nutrients such as phosphate. The formation of single mineralogy cements can be rare in natural sedimentary systems. Even using pure cultures under controlled conditions, we found mixed mineralogy in some samples (as in sample C-3:1 and C-Alt-SW) that may be due to the unknown growth behavior of the microbes – where the sulfate reducing bacteria re-grew after the first precipitation event (please refer to online supplementary material for detailed growth curve and pH data). The re-growth further increases the alkalinity and lead to a second supersaturation but at a much higher Mg/Ca ratio, causing a precipitation of a different calcium carbonate polymorph than the initial precipitation. In closed or semi-closed marine sediment, it is very likely that the growth cycle of microbes might change over time as a function of food source availability, leads to multiple precipitation events and also mixed mineralogy of the precipitated minerals.

5.0 CONCLUSION AND IMPLICATIONS

In conclusion, microbial sulfate reduction is capable of driving precipitation of calcium carbonate polymorphs via metabolic activities that change the solution chemistry. Bacterial cells can act as effective nucleation surfaces for calcium carbonate polymorphs to grow. The cellular materials are often a better substrate compared to calcite and kaolinite seeds, which likely results from the combined effects of surface energetics and local perturbations to solution chemistry proximal to actively metabolising cells. This also implies that heterogenous precipitation is a dominant precipitation pathway in sediments that host sulfate reducing bacteria. Under a closed and active system, calcium carbonate polymorphs selection depends on the solution chemistry at the time of nucleation, even though the solution chemistry might then evolve. Several variables influence calcium carbonate polymorphism via microbial sulfate reduction under a closed system: Mg/Ca >> PO_4^{3-} >>

847 SO_4^{2-} and the type of seeding materials. The growth of magnesium calcite is promoted in
848 experiments with calcite seeds which, in turn, influences the apparent stability domain
849 between calcite and MHC in the present of calcite and kaolinite seeds. Our biotic-mediated
850 spherulitic MHC comprises a unique hollow cavity with calcified microbes texture. The
851 texture is absence in abiotic experiments, thus, may hold implications for sedimentary
852 geologists to interpret abiotic and biotic signatures of precipitated minerals in the
853 environment. Nevertheless, our transformation experiment suggests that such microbial
854 texture/signature could be vulnerable to diagenetic processes in the environment. Results
855 from biotic, abiotic and transformation experiments showed that phosphate stabilizes MHC,
856 while retarding the formation of aragonite and calcite at Mg/Ca > 2. We also found that
857 phosphate concentrations have a lesser effect on which polymorph initially precipitates. In
858 the presence of high phosphate concentrations, MHC formed instead of aragonite because
859 phosphate ions inhibit the nucleation of aragonite. Therefore, we suggest that caution
860 should be taken when interpreting the types of calcium carbonate polymorphs formed in
861 biotic studies that uses yeast extract or any additives that has phosphorus content. Similar
862 claim applies to environmental samples where metastable MHC is particularly prone to
863 diagenetic processes. Thus, care should be taken while interpreting environmental samples
864 as any transformation processes of MHC can have detrimental effect on paleo proxy such as
865 isotopic signature or Mg/Ca in the sedimentary carbonates.
866
867 **ACKNOWLEDGEMENT**
868 The authors would like to acknowledge the funding for this research ERC StG 307582 to AVT
869 (CARBONSINK). CYL would also like to thank the Ministry of Education Malaysia for the SLAI
870 (Skim Latihan Akademik IPTA) scholarship and Universiti Malaya for providing the study
871 leave. The authors are also indebted to Tony Dickson, Harold Bradbury, Gilad Antler, and Jo
872 Clegg for their discussion and assistant in the laboratory.
873
874 **SUPPLEMENTARY MATERIALS**
875
876 **REFERENCES**
877 Aloisi G. Gloter A. Kruger M. Wallmann K. Guyot F. and Zuddas P. (2006) Nucleation of
878 calcium carbonate on bacterial nanoglobules. *Geology* **34**(12), 1017 – 1020.

879 Althoff P.L. (1977) Structural refinements of dolomite and a magnesian calcite and
880 implications for dolomite formation in the marine environment. *Am. Mineral*. **62**, 772 – 783.
881 Arias D. Cisternas L.A. and Rivas M. (2017) Biomineralization of calcium and magnesium
882 crystals from seawater by halotolerant bacteria isolated from Atacama Salar (Chile).
883 *Desalination*. **405**, 1 – 9.
884 Balci N. Menekse M. Karaguler N.G. Sonmez M.S. and Meister P. (2016) Reproducing
885 authigenic carbonate precipitation in the hypersaline Lake Acigol (Turkey) with microbial
886 cultures. *Geomicrobiol J*. **33**(9), 758 – 773.
887 Baumgartner L.K. Dupraz C. Buckley D.H. Spear J.B. Pace N.R. and Visscher P.T. (2009)
888 Microbial species richness and metabolic activities in hypersaline microbial mats: Insight
889 into biosignature formation through lithification. *Astrobiol*. **9**(9), 861 – 874.
890 Berner R.A. Scott M.R. and Thomlinson C. (1970) Carbonate alkalinity in the pore waters of
891 anoxic marine sediments. *Limnol. Oceanography*. **15**(4), 544 – 549.
892 Berner R.A. (1975) The role of magnesium in the crystal growth of calcite and aragonite
893 from seawater. *Geochim. Cosmochim. Acta*. **39**, 489 – 504.
894 Berner R.A. and Morse J.W. (1974) Dissolution kinetics of calcium carbonate in seawater. IV.
895 Theory of calcite dissolution. *Am. J. Sci*. **274**, 108 – 134.
896 Blue C.R. Giuffre A. Mergelsberg S. Han N. De Yoreo J.J. and Dove P.M. (2017) Chemical and
897 physical controls on the transformation of amorphous calcium carbonate into crystalline
898 $CaCO_3$ polymorphs. *Geochim. Cosmochim. Acta*. **196**, 179 – 196.
899 Bosak T. and Newman D.K. (2005) Microbial kinetic controls on calcite morphology in
900 supersaturated solutions. *J. Sedimentary Res*. **75**(2), 190 – 199.
901 Bots P. Benning L.G. Rickaby R.E.M. and Shaw S. (2011) The role of SO_4 in the switch from
902 calcite to aragonite seas. *Geology.* **39**, 331 – 334.
903 Bots P. Benning L.G. Rodriguez-Blanco J.D. Roncal-Herrero R.T. and Shaw S. (2012)
904 Mechanistic insights into the crystallization of amorphous calcium carbonate (ACC). *Crystal*
905 *Growth Design.* **12**, 3806 – 3814.
906 Braissant O. Decho A.W. Dupraz C. Glunk C. Przekop K.M. and Visscher P.T. (2007)
907 Exopolymeric substances of sulfate reducing bacteria: Interactions with calcium at alkaline
908 pH and implication for formation of carbonate minerals. *Geobiology*. **5**, 401 – 411.
909 Brecevic L. and Nielsen A.E. (1989) Solubility of amorphous calcium carbonate. *J. Crystal*
910 *Growth*. **98**(3), 504 – 510.

911 Brönsted J.N. (1922) Studies on solubility. IV. The principle of the specific interaction of ions.
912 *J. Am. Chem. Soc*. **44**, 877 – 898.
913 Brooks R. Clack L.M. and Thurston E.F. (1950) Calcium carbonate and its hydrates. *Phil. Trans.*
914 *Royal Soc. A*. **243**, 145 – 167.
915 Burdige D.J. (1991) The kinetics of organic matter mineralization in anoxic marine sediments.
916 *J. Mar. Res*. **49**, 727 – 761.
917 Burton E.A. and Walter L.M. (1990) The role of pH in phosphate inhibition of calcite and
918 aragonite precipitation rates in seawater. *Geochim Cosmochim Acta*. **54**, 797 – 808.
919 Burton E.A. (1993) Controls on marine carbonate cement mineralogy: review and
920 reassessment. *Chem Geol*. **105**, 163 – 179.
921 Busenberg E. and Plummer N.L. (1985) Kinetics and thermodynamic factors controlling the
922 distribution of SO_4^{2-} and Na^+ in calcites and selected aragonites. *Geochim. Cosmochim. Acta*.
923 **49**, 713 – 725.
924 Chafetz H. Barth J. Cook M. Guo X. and Zhou J. (2018). Origins of carbonate spherulites:
925 Implications for Brazilian Aption pre-salt reservoir. *Sed. Geol*. **365**, 21 – 33.
926 Chen L. Shen Y. Xie A. Huang B. Jia R. Guo R. and Tang W. (2009) Bacteria-mediated
927 synthesis of metal carbonate minerals with unusual morphologies and structures. *Crystal*
928 *Growth Design*. **9**(2), 743 – 754.
929 Christ C.L. and Hostetle P.B. (1970) Studies in system MgO – SiO_2 – CO_2 – H_2O. (II) Activity-
930 product constant of magnesite. *Am. J. Sci*. **268**(5), 439 – 453.
931 Coelho W.A. (2007) *TOPAS-Academic, Coelho Software*. Brisbane, Australia.
932 Coleman M.L. Hedrick D.B. Lovley D.R. White D.C. and Pye K. (1993) Reduction of Fe(III) in
933 sediments by sulfate reducing bacteria. *Nature*. **361**, 436 – 438.
934 Dahl K. and Buchardt B. (2006) Monohydrocalcite in the arctic Ikka Fjord, SW Greenland:
935 First reported marine occurrence. *J. Sedimentary Res*. **76**, 460 – 471.
936 de Choudens-Sanchez V. and Gonzalez L.A. (2009) Calcite and aragonite precipitation under
937 controlled instantaneous supersaturation: Elucidating the role of $CaCO_3$ saturation state and
938 Mg/Ca ratio on calcium carbonate polymorphism. *J. Sedimentary Res*. **79**, 363 – 376.
939 De Kanel J. and Morse J.W. (1978) The chemistry of orthophosphate uptake from seawater
940 on to calcite and aragonite. *Geochim. Cosmochim Acta*. **42**, 1335 – 1340.
941 De Yoreo J.J. Filbert P.U.P.A. Sommerdijk N.A.J.M. Lee Penn R. Whitelam S. Joester D. Zhang
942 H. Rimer J.D. Navrotsky A. Banfield J.F. Wallace A.F. Michel F.M. Meldrum F.C. Colfen H. and

943 Dove P.M. (2015) Crystallization by particle attachment in synthetic, biogenic, and geologic
944 environments. *Science*. **349**(6247). Doi 10.1126/science.aaa6760.
945 Dejehet F. Idrissi S. and Debuyst R. (1999) Magnesium and occluded water in calcium
946 carbonate monohydrate. *J. de Chimie Physique*. **96**, 741 – 753.
947 Delaney M.L. (1998) Phosphorus accumulation in marine sediments and the oceanic
948 phosphorus cycle. *Global Biogeochem. Cycle*. **12**(4), 563 – 572.
949 Dickson A.G. Afghan J.D. and Anderson G.C. (2003) Reference materials for oceanic CO_2
950 analysis: a method for the certification of total alkalinity. *Mar. Chem*. **80**(2-3), 185 – 197.
951 Dickson J.A.D. (1993) Crystal growth diagrams as an aid to interpreting the fabrics of calcite
952 aggregates. *J. Sedimentary Res*. **63**(1), 1 – 17.
953 Dupraz C. Reid R.P. Braissant O. Decho A.W. Norman R.S. and Visscher P.T. (2009) Processes
954 of carbonate precipitation in modern microbial mats. *Earth Sci. Rev*. **96**, 141 – 162.
955 Edmund Wajon J. Ho G-E. and Murphy P.J. (1985) Rate of precipitation of ferrous iron and
956 formation of mixed iron-calcium carbonates by naturally occurring carbonate materials.
957 *Water Res*. **19**(7), 831 – 837.
958 Egger M. Jilbert T. Behrends T. Rivard C. and Slomp C.P. (2015). Vivianite is a major sink for
959 phosphorus in methanogenic coastal surface sediments. *Geochim. Cosmochim. Acta*. **169**,
960 217 – 235.
961 Elstnerova P. Friak M. Fabritius H.O. Lymperakis L. Hickel T. Petrov M. Nikolov S. Raabe D.
962 Ziegler A. Hild S. and Neugebauer J. (2010) *Acta Biomaterialia*. **6**(10), 4506 – 4512.
963 Faul K.L. Paytan A. and Delaney M.L. (2005) Phosphorus distribution in sinking oceanic
964 particulate matter. *Mar. Chem*. **97**(3 – 4), 307 – 333.
965 Fukushi K. Munemoto T. Sakai M. and Yagi S. (2011) Monohydrocalcite: a promising
966 remediation material for hazardous anions. *Sci. Technol. Adv. Materials*. **12**, 64702 – 64714.
967 Fukushi K. Suzuki Y. Kawano J. Ohno T. Ogawa M. Yaji T. and Takahashi Y. (2017) Speciation
968 of magnesium in monohydrocalcite: XANES, *ab initio* and geochemical modelling. *Geochim.*
969 *Cosmochim. Acta*. **213**, 457 – 474.
970 Gallagher K.L. Kading T.J. Braissant O. Dupraz C. and Visscher P.T. (2012) Inside the alkalinity
971 engine: the role of electron donors in the organomineralization potential of sulfate-reducing
972 bacteria. *Geobiol*. **10**(6), 518 – 530.
973 Gallagher K.L. Braissant O. Kading T.J. Dupraz C. and Visscher P.T. (2013) Phosphate-related
974 artifacts in carbonate mineralization experiments. J. Sed. Res. **83**, 37 – 49.

975 Granasy L. Pusztai T. Tegze G. Warren J.A. Douglas J.F. (2005) Growth and form of
976 spherulites. *Phys. Rev. Let*. **72**, 011605.
977 Grases F. and March J.G. (1990) Determination of phosphate based on inhibition of crystal
978 growth of calcite. *Anal. Chim. Acta*. **229**, 249 – 254.
979 Guggenheim E.A. and Turgeon J.C. (1955) Specific interaction of ions. *Trans. Faraday Soc*. **51**,
980 747 – 761.
981 Han Z. Li D. Zhao H. and Yan Li P. (2017) Precipitation of carbonate minerals induced by the
982 halophilic *Chromohalobacter Israelensis* under high salt concentrations: Implications for
983 natural environments. *Minerals*. **7**(6), 95; doi:103390/min7060095.
984 Han M. Zhao Y. Zhao H. Han Z. Yan H. Sun B. Meng R. Zhuang D. Li D. and Liu B. (2017a). A
985 comparison of amorphous calcium carbonate crystallization in aqueous solutions of $MgCl_2$
986 and $MgSO_4$: implications for paleo-ocean chemistry. *Mineral. Petrol*. DOI 10.1007/s00710-
987 017-0528-9. pp 1 – 16.
988 Haouari O. Fardeau M.L. Casalot L. Tholozan J.L. Hamdi M. and Ollivier B. (2006) Isolation of
989 sulfate-reducing bacteria from Tunisian marine sediments and description of *Desulfovibrio*
990 *bizertensis* sp. nov. *Int. J. System. Evol. Microbiol*. **56**, 2909 – 2913.
991 Hood A.V.S. Wallace M.W. and Drysdale R.N. (2011) Neoproterozoic aragonite-dolomite
992 seas? Widespread marine dolomite precipitation in Cryogenian reef complexes. *Geology*. **9**,
993 871 – 874.
994 Hopkinson L. Kristova P. Rutt K. and Cressey G. (2012) Phase transitions in the system MgO-
995 CO_2-H_2O during CO_2 degassing of Mg-bearing solutions. *Geochim. Cosmochim. Acta*. **76**, 1 –
996 13.
997 Hull H. and Turnbull A.G. (1973) A thermodynamic study of monohydrocalcite. *Geochim.*
998 *Cosmochim. Acta*. **37**, 685 – 694.
999 Hyacinthe C. and Van Cappellen (2004). An authigenic iron phosphate phase in estuarine
1000 sediments: composition, formation and chemical reactivity. *Mar. Chem*. **91**, 227 – 251.
1001 Ihli J. Wong W.C. Noel E.H. Kim Y.Y. Kulak A.N. Christenson H.K. Duer M.J. and Meldrum F.C.
1002 (2014) Dehydration and crystallization of amorphous calcium carbonate in solution and in
1003 air. *Nature Comm*. **5**(3169), 1 – 10.
1004 Kamiya K. Sakka S. and Terada K. (1977) Aragonite formation through precipitation of
1005 calcium carbonate monohydrate. *Materials Res. Bull*. **12**(11), 1095 – 1102.

1006 Katz A. (1973). The interaction of magnesium with calcite during crystal growth at 25 – 90˚C
1007 and one atmosphere. *Geochim. Cosmochim. Acta*. **37**, 1563 – 1586.
1008 Kawaguchi T. and Decho A.W. (2002) A laboratory investigation of cyanobacterial
1009 extracellular polymeric secretions (EPS) in influencing $CaCO_3$ polymorphism. *J. Crystal*
1010 *Growth*. **240**, 230 – 235.
1011 Kraal P. Slomp C.P. Reed D.C. Reichart G.J. and Poulton S.W. (2012) Sedimentary phosphorus
1012 and iron cycling in and below the oxygen minimum zone of the northern Arabian Sea.
1013 *Biogeosciences*. **9**, 2603 – 2624.
1014 Kimura T. and Koga N. (2011) Monohydrocalcite in comparison with hydrated amorphous
1015 calcium carbonate: Precipitation condition and thermal behaviour. *Crystal Growth Design*.
1016 **11**, 3877 – 3884.
1017 Kipp M.A. and Stueken E.E. (2017) Biomass recycling and Earth's early phosphorus cycle. *Sci.*
1018 *Adv*. **3**, eaao4795, 1 – 6.
1019 Kitson R.E. and Mellon M.G. (1944) Colorimetric determination of phosphorus as
1020 molybdovanadophosphoric acid. *Indus. Engin. Chem. Res*. **16**, 379.
1021 Lenders J.J. Dey A. Bomans P.H.H. Spielmann J. Hendrix M.M.R.M. de With G. Meldrum F.C.
1022 Harder D. and Sommerdijk N.A.J.M. (2012) High-magnesian calcite mesocrystals: A
1023 coordination chemistry approach. *J. Am. Soc*. **134**, 1367 – 1373.
1024 Lippmann F. (1973) *Sedimentary Carbonate Minerals*. Springer Verlag, Berlin Heidelberg.
1025 Lin Y.P. and Singer P.C. (2005) Inhibition of calcite crystal growth by polyphosphates. *Water*
1026 *Res*. **39**(19). 4835 – 4843.
1027 Lin C.J. Yang S.Y. Huang S.J. and Chan J.C.C. (2015) Structural characterization of Mg-
1028 stabilized amorphous calcium carbonate by Mg-25 solid-state NMR spectroscopy. *J. Phys.*
1029 *Chem. C*. **119**, 7225 – 7233.
1030 Lioliou M.G. Paraskeva C.A. Koutsoukos P.G. and Payatakes A.C. (2007) Heterogeneous
1031 nucleation and growth of calcium carbonate on calcite and quartz. *J. Colloid Interface Sci*.
1032 **208**, 421 – 428.
1033 Liu R. Liu F.L. Zhao S.Q. Su Y.L. Wang D.J. and Shen Q. (2013) Crystallization and oriented
1034 attachment of monohydrocalcite and its crystalline phase transformation. *Cryst. Engin.*
1035 *Comm*. **15**, 509 – 515.

1036 Loste E. Wilson R.M. Seshadri R. and Meldrum F.C. (2003) The role of magnesium in
1037 stabilizing amorphous calcium carbonate and controlling calcite morphologies. *J. Crystal*
1038 *Growth*. **254**, 206 – 218.
1039 Madsen I.C. and Scarlett N.V.Y. (2008) Quantitative Phase Analysis. In *Powder Diffraction:*
1040 *Theory and Practice* (eds by Dinnabier, R.E.). Royal Society of Chemistry.
1041 Marschner H. (1969) Hydrocalcite ($CaCO_3.H_2O$) and Nesquehonite ($MgCO_3.3H_2O$) in
1042 carbonate scales. *Science*. **165**, 1119 – 1121.
1043 McCusker L.B. Von Dreele R.B. Cox D.E. Louer D. Scardi P. (1999) Reitveld refinement
1044 guidelines. *J. Appl. Crystallography*. **32**(1), 36 – 50.
1045 Meic I.B. Kontec J. Jurasin D.D. Dzakula B.N. Stajner L. Lyons D.M. Sikiric M.D. and Kralj D.
1046 (2017) Comparative study of calcium carbonates and calcium phosphates precipitation in
1047 model systems mimicking the inorganic environment for biomineralization. *Crystal Growth*
1048 *Design*. **17**(3), 1103 – 1117.
1049 Meister P. (2013) Two opposing effects of sulfate reduction on carbonate precipitation in
1050 normal marine, hypersaline, and alkaline environments. *Geology*. **41** (4), 499 – 502.
1051 Morse J.W. (1974) Dissolution kinetics of calcium carbonate in sea water. V. Effects of
1052 natural inhibitors and the position of chemical lysocline. *Am. J. Sci*. **274**, 638 – 647.
1053 Morse J.M. and He S. (1993) Influences of T, S and P_{CO2} on the pseudo-homogeneous
1054 precipitation of $CaCO_3$ from seawater: implications for whiting formation. *Mar. Chem*. **41**,
1055 291 – 297.
1056 Munemoto T. and Fukushi K. (2008) Transformation kinetics of monohydrocalcite to
1057 aragonite in aqueous solutions. *J. Mineral. Petrol. Sci*. **103**, 345 – 349.
1058 Munemoto T. Fukushi K. Kanzaki Y. and Murakami T. (2014) Redistribution of Pb during
1059 transformation of monohydrocalcite to aragonite. *Chem. Geol*. **387**, 133 – 143.
1060 Nishiyama R. Munemoto T. and Fukushi K. (2013) Formation condition of monohydrocalcite
1061 from $CaCl_2$-$MgCl_2$-Na_2CO_3 solutions. *Geochim. Cosmochim. Acta*. **100**, 217 – 231.
1062 Nielsen M.R. Sand K.K. Rodgriguez-Blanco J.D. Bovet N. Generosi J. Dalby K.K. and Stipp S.L.S.
1063 (2016) Inhibition of calcite growth: Combined effects of Mg^{2+} and SO_4^{2-}. *J. Crystal Growth*. **16**,
1064 6199 – 6207.
1065 Obst M. Dynes J.J. Lawrence J.R. Swerhone G.D.W. Benzerara K. Karunakaran C. Kaznatcheev
1066 K. Tyliszczak T. and Hitchcock A.P. (2009) Precipitation of amorphous $CaCO_3$ (aragonite-like)

by cynobacteria: A STXM study of the influence of EPS on the nucleation process. *Geochim. Cosmochim. Acta*. **73**, 4180 – 4198.

Omoike A. and Chorover J. (2006) Adsorption to goethite of extracellular polymeric substances from *Bacillus subtilis*. *Geochem. Cosmochim. Acta*. **70**, 827 – 838.

Oomori T. Kyan A. and Kitano Y. (1988) Magnesium calcite synthesis from calcium bicarbonate solution containing magnesium ions in the presence of fluoride and phosphate ions. *Geochem. J*. **22**, 275 – 283.

Picard A. Gartman A. Clarke D.R. and Girguis P.R. (2018) Sulfate-reducing bacteria influence the nucleation and growth of mackinawite and greigite. *Geochim. Cosmochim. Acta*. **220**, 367 – 384.

Plummer L.N. and Busenberg E. (1982) The solubilities of calcite, aragonite and vaterite in CO_2 – H_2O solutions between 0 and 90˚C, and an evaluation of the aqueous model for the system $CaCO_3$-CO_2-H_2O. *Geochim. Cosmochim. Acta*. **46**(6), 1011 – 1040.

Politi Y. Arad T. Klein E. Weiner S. and Addadi L. (2004) Sea urchin spine calcite forms via a transient amorphous calcium carbonate phase. *Science.* **306**, 1161 – 1164.

Purgstaller B. Konrad F. Dietzel M. Immenhauser A. and Mavromatis V. (2017) Control of Mg^{2+}/Ca^{2+} activity ratio on the formation of crystalline carbonate minerals via an amorphous precursor. *Crystal Growth Design*. **17**, 1069 – 1078.

Pye K. Dickinson A.D. Schiavon N. Coleman M.L. and Cox M. (1990). Formation of siderite-Mg-calcite iron sulphide concretions in intertidal marsh and sandflat sediments, north Norfolk, England. *Sedimentology*. **37**, 325 – 343.

Qiu X. Yao Y. Wang H. and Duan Y. (2017) Live microbial cells adsorb Mg^{2+} more effectively than lifeless organic matter. *Frontiers Earth Sci*. DOI 10.1007/s11707-017-0626-3.

Raiswell R. and Fisher Q.J. (2004) Rates of carbonate cementation associated with sulfate reduction in DSDP/ODP sediments: Implications for the formation of concretions. *Chem. Geol*. **211**, 71 – 85.

Ries J.B. Anderson M.A. and Hill R.T. (2008) Seawater Mg/Ca controls polymorph mineralogy of microbial $CaCO_3$: A potential proxy for calcite-aragonite seas in Precambrian time. *Geobiology*. **6**, 106 – 119.

1097 Rivadeneyra M.A. Delgado G. Ramos-Cormenzana A. and Delgado R. (1998)
1098 Biomineralization of carbonates by *Halomonas eurihalina* in solid and liquid media with
1099 different salinities: crystal formation sequence. *Res. Microbiol*. **149**(4), 227 – 287.
1100 Rivadeneyra M.A. Martin-Algarra A. Sanchez-Roman M. Sanchez-Navas A. Martin-Ramos J.D.
1101 (2010) Amorphous Ca-phosphate precursors for Ca-carbonate biominerals mediated by
1102 Chromohalobacter marismortui. *ISME J*. **4**, 922 – 932.
1103 Rodriguez-Blanco J.D. Shaw S. Bots P. Roncal-Herrero T. Benning L.G. (2014) The role of Mg
1104 in the crystallization of monohydrocalcite. *Geochim. Cosmochim. Acta*. **127**, 204 – 220.
1105 Rodriguez-Navarro C. Jroundi F. Schiro M. Ruiz-Agdo E. and Gonzalez-Munoz M.T. (2012)
1106 Influence of substrate mineralogy on bacterial mineralization of calcium carbonate:
1107 Implications for stone conservation. *Appl Environ Microbiol*. **78** (11), 4017 – 4029.
1108 Rodriguez-Blanco J.D. Sand K.K. and Benning L.G. (2017) ACC and vaterite as intermediates
1109 in the solution-based crystallization of $CaCO_3$. In A.E.S. Van Driessche et al. (eds.), *New*
1110 *Perspectives on Mineral Nucleation and Growth.* DOI10.1007/978-3-319-45669-0_5.
1111 Sanchez-Navas A. Martin-Algarra A. Rivadeneyra M.A. Melchor S. Martin-Ramos J.D. (2009)
1112 Crystal-growth behaviour in Ca-Mg carbonate bacterial spherulites. *Crystal Growth Design*.
1113 **9**(6), 2690 – 2699.
1114 Sanchez-Roman M. Rivadeneyra M.A. Vasconcelos C. McKenzie J.A. (2007).
1115 Biomineralization of carbonate and phosphate by moderately halophilic bacteria. *FEMS*
1116 *Microbiol. Ecol*. **61**, 273 – 284.
1117 Sasaki K. Noriki S. and Tsunogai S. (2001) Vertical distributions of interstitial phosphate and
1118 fluoride in anoxic sediment: Insight into the formation of an authigenic fluoro-phosphorus
1119 compound. *Geochem. J*. **35**, 295 – 306.
1120 Sinkko H. Lukkari K. Sihvonen L.M. Sivonen K. Leivuori M. Rantanen M. Paulin L. and Lyra C.
1121 (2013) Bacteria contribute to sediment nutrient release and reflect progressed
1122 eutrophication driven hypoxia in an organic-rich continental sea. *PLoS ONE*. **8**(6), e67061.
1123 Doi:10.1371/journal.pone.0067061.
1124 Smeets P.J.M. Cho K.R. Kempen R.G.E. Sommerdijk N.A.J.M. and De Yoreo J.J. (2015)
1125 Calcium carbonate nucleation driven by ion binding in a biomimetic matrix revealed by *in*
1126 *situ* electron microscopy. *Nature Materials*. **14**, 394 – 399.
1127 Soetaert K. Hofmann A. Middleberg J. Meysman F. and Greenwood J. (2007). The effect of
1128 biogeochemical processes on pH. *Mar. Chem*. **105**, 30 – 51.

1129 Steiner Z. Rapaport H. Oren Y. and Kasher R. (2010). Effect of surface-exposed chemical
1130 groups on calcium-phosphate mineralization in water treatment system. Env. Sci. Technol.
1131 **44**, 7937 – 7943.
1132 Stockmann G. Tollefsen E. Skelton A. Bruchert V. Balic-Zunic T. Langhof J. Skogby H. and
1133 Karlsson A. (2018) Control of a calcite inhibitor (phosphate) and temperature on ikaite
1134 precipitation in Ikka Fjord, southwest Greenland. *Appl. Geochem.* **89**, 11 – 22.
1135 Stoffers P. and Fischbeck R. (1974) Monohydrocalcite in the sediments of Lake Kivu (East
1136 Africa). *Sedimentology*. **21**, 163 – 170.
1137 Sun W. Jayaraman S. Chen W. Persson K.A. and Ceder G. (2015) Nucleation of metastable
1138 aragonite $CaCO_3$ in seawater. *Proc. Nat. Acad. Sci*. **112**(11), 3199 – 3204.
1139 Suzuki M. Nagasawa H. and Kogure T. (2006) Synthesis and structure of hollow calcite
1140 particles. *Crystal Growth Design*. **6**(9), 2004 – 2006.
1141 Tadier S. Rokidi S. Rey C. Combes C. and Koutsoukos P.G. (2017) Crystal growth of aragonite
1142 in the presence of phosphate. *J. Crystal Growth*. **458**, 44 – 52.
1143 Taylor G.F. (1975) The occurrence of monohydrocalcite in two small lakes in the South-East
1144 of South Australia. *Am. Mineral*. **60**, 690 – 697.
1145 Teller J.T. and Last W.M. (1990) Paleohydrological indicators in playas and salt lakes, with
1146 examples from Canada, Australia, and Africa. *Paleogeo. Paleoclim. Paleoecol*. **76**, 215 – 240.
1147 Tracy S.L. Williams D.A. and Jennings H.M. (1998) The growth of calcite spherulites from
1148 solution II. Kinetics of formation. *J. Crystal Growth*. **193**, 382 – 388.
1149 Tommaso D.D. and de Leeuw N.H. (2010) Structure and dynamics of the hydrated
1150 magnesium ion and of the solvated magnesium carbonates: insights from first principles
1151 simulations. *Phys. Chem. Chem. Phys*. **12**, 894 – 901.
1152 Tourney J. and Ngwenya B.T. (2009) Bacterial extracellular polymeric substances (EPS)
1153 mediate $CaCO_3$ morphology and polymorphism. *Chem. Geol*. **262**, 138 – 146.
1154 van Lith Y. (2001) *The role of sulfate reducing bacteria in dolomite formation. Study of a*
1155 *recent environment, bacterial cultures, and dolomite concretions*. PhD thesis.
1156 Visscher P.T. Reid R.P. and Bebout B.M. (2000) Microscale observations of sulfate reduction:
1157 Correlation of microbial activity with lithified micritic laminae in modern marine
1158 stromatolites. *Geology*. **28**(10), 919 – 922.
1159 Visscher P.T. and Stolz, J.F. (2005) Microbial mats as bioreactors: Populations, processes,
1160 and products. Paleogeo. Paleoclim. Paleoecol. **219**, 87 – 100.

1161 Wacey D. Wright D.T. and Boyce A.J. (2007) A stable isotope study of microbial dolomite
1162 formation in the Coorong Region, South Australia. *Chem. Geol*. **244**, 155 – 174.
1163 Walter L.M. (1986) Relative efficiency of carbonate dissolution and precipitation during
1164 diagenesis: a progress report on the role of solution chemistry. In Gautier, D.L., ed., *Roles of*
1165 *organic matter in sediment diagenesis*: Soc. Econ. Pal. Min. Sp. Pub. 38, p. 1 – 11.
1166 Walter L.K. and Burton E.A. (1986) The effect of orthophosphate on carbonate mineral
1167 dissolution rates in seawater. *Chem. Geol*. **56**, 313 – 323.
1168 Warthmann R. van Lith Y. Vasconcelos C. McKenzie J.A. and Karpoff A.M. (2000) Bacterially
1169 induced dolomite precipitation in anoxic culture experiments. *Geology*. **28**(12), 1091 – 1094.
1170 Wolf S.L. Jahme K. and Gebauer D. (2015) Synergy of Mg^{2+} and poly(aspartic acid) in
1171 additive-controlled calcium carbonate precipitation. *Cryst. Engin. Comm*. **17**, 6857 – 6862.
1172 Xu J. Yan C. Zhang F. Konishi H. Xu H. and Teng H.H. (2013) Testing the cation-hydration
1173 effect on the crystallization of Ca-Mg-CO_3 systems. *Proc. Nat. Acad. Sci.* **110**(44), 17750 –
1174 17755
1175 Yagi S. and Fukushi K. (2011) Phosphate sorption on monohydrocalcite. *J. Mineral. Petrol. Sci.*
1176 **106**, 109 – 113.
1177 Zhu, T. and Dittrich M. (2016) Carbonate precipitation through microbial activities in natural
1178 environment, and their potential in biotechnology: A review. *Frontiers Bioengin. Biotechnol*.
1179 **4**(4), 1 – 21.